Contrib Mineral Petrol (2010) 159:1–24
DOI 10.1007/s00410-009-0412-7

ORIGINAL PAPER

Titanium in phengite: a geobarometer for high temperature eclogites

Estelle Auzanneau · M. W. Schmidt · D. Vielzeuf · J. A. D Connolly

Received: 4 July 2008 / Accepted: 13 May 2009 / Published online: 12 June 2009

Abstract Phengite chemistry has been investigated in experiments on a natural SiO_2–TiO_2-saturated greywacke and a natural SiO_2–TiO_2–Al_2SiO_5-saturated pelite, at 1.5–8.0 GPa and 800–1,050°C. High Ti-contents (0.3–3.7 wt %), Ti-enrichment with temperature, and a strong inverse correlation of Ti-content with pressure are the important features of both experimental series. The changes in composition with pressure result from the Tschermak substitution ($Si + R^{2+} = Al^{IV} + Al^{VI}$) coupled with the substitution: $Al^{VI} + Si = Ti + Al^{IV}$. The latter exchange is best described using the end-member Ti-phengite ($KMgTi[Si_3Al]O_{10}(OH)_2$, TiP). In the rutile-quartz/coesite saturated experiments, the aluminoceladonite component increases with pressure while the muscovite, paragonite and Ti-phengite components decrease. A thermodynamic model combining data obtained in this and previous experimental studies are derived to use the equilibrium MgCel + Rt = TiP + Cs/Qz as a thermobarometer in felsic and basic rocks. Phengite, rutile and quartz/coesite are common phases in HT-(U)HP metamorphic rocks, and are often preserved from regression by entrapment in zircon or garnet, thus providing an opportunity to determine the *T*–*P* conditions of crystallization of these rocks. Two applications on natural examples (Sulu belt and Kokchetav massif) are presented and discussed. This study demonstrates that Ti is a significant constituent of phengites that could have significant effects on phase relationships and melting rates with decreasing *P* or increasing *T* in the continental crust.

Keywords Phengite · Titanium · Thermodynamic modelling · Thermobarometry · UHP metamorphism

Communicated by J. Blundy.

Electronic supplementary material The online version of this article (doi:10.1007/s00410-009-0412-7) contains supplementary material, which is available to authorized users.

E. Auzanneau (✉) · M. W. Schmidt · J. A. D Connolly
Institute for Mineralogy and Petrology,
ETH, 8092 Zurich, Switzerland
e-mail: estellea75@gmail.com

E. Auzanneau
Laboratoire Magmas et Volcans, OPGC, CNRS et Université Blaise Pascal, 5 rue Kessler, 63038 Clermont-Ferrand, France

D. Vielzeuf
CINaM, CNRS, Aix-Marseille University, Campus de Luminy, 13288 Marseille, France

Introduction

Potassic micas are common minerals in crustal metamorphic rocks. Titanium is one of the most important minor elements in both trioctahedral biotite and dioctahedral muscovite or phengite. The behaviour of titanium in biotite, and the effects on its stability conditions are well known. Ti-contents increase with temperature (Robert 1975, 1976; Guidotti et al. 1977) and can be used to estimate the temperature of crystallisation (Henry et al. 2005). Biotite coexisting with a Ti-oxide is richer in Ti (Montel and Vielzeuf 1997), and titanium extends the biotite stability limit to higher temperatures (Dymek 1983; Guidotti 1984; Stevens et al. 1997). This latter effect has consequences on fluid-absent melting processes because biotite is the main H_2O-bearing mineral at low pressure and high temperature in crustal rocks (Vielzeuf and Montel 1994; Stevens et al. 1997; Nair and Chacko 2002).

In contrast, the behaviour of titanium in white mica remains unclear. Until the early 1990s, titanium contents in potassic white mica were considered as too low to have a

significant effect on metamorphic reactions (Guidotti 1984). Later on, on the basis of studies reporting Ti- and Si-rich potassic white mica (Biino and Compagnoni, 1992; Vavilov et al. 1991; Snoeyenbos et al. 1995), Guidotti and Sassi (1998a) and Guidotti and Sassi (1998b) concluded that "high Ti-values seemed to be related to a combination of both very high P and high T" ($P > 1.5$–3 GPa; $T = 700$–1,000°C). This idea has not yet been confirmed and the effects of titanium on potassic white mica stability, phase relationships, and fluid-absent melting remain to be clarified. A recent experimental study reports a change of Ti in phengite with P and T (Hermann and Spandler 2008). However, additional data are required to determine both the variation of the Ti-content as a function of P and T and the substitution mechanisms involving Ti in phengite. In this study, we experimentally determine the chemical changes of phengite as a function of P and T, investigate the behaviour and the substitution of Ti, and calibrate a geobarometer based on the Ti content in phengite for quartz/coesite + rutile saturated rocks.

Experimental and analytical techniques

Starting material

Two natural samples have been investigated: a meta-greywacke (CEVP) composed of quartz, plagioclase and biotite, and an Al_2SiO_5-saturated metapelite (CO) composed of quartz, plagioclase, kyanite, muscovite, biotite and garnet. Their bulk compositions differ mainly in Al_2O_3, FeO and Na_2O concentrations (Table 1). The starting materials have already been used in previous studies for other purposes (Vielzeuf and Holloway 1988; Vielzeuf and Montel 1994; Montel and Vielzeuf 1997; Schmidt et al. 2004; Auzanneau et al. 2006) and they have been described in detail by Vielzeuf and Montel (1994) and Vielzeuf and Holloway (1988), respectively.

Table 1 Starting material compositions

	CEVP	CO
SiO_2	69.990	64.35
Al_2O_3	12.960	18.13
FeO[a]	4.820	6.26
MgO	2.360	2.44
MnO	0.060	0.09
CaO	1.670	1.52
Na_2O	2.950	1.66
K_2O	2.410	2.56
TiO_2	0.700	0.82
P_2O_5	0.200	–
H_2O	1.430	2.15
Total	99.350	99.98

[a] All iron as FeO

Experimental techniques

Experiments have been performed employing a fine powder (≤5 μm), dried at 110°C, and placed in thin-walled Au-capsules, which were then welded shut. Depending on temperature, the experiments lasted between 1 and 15 days. Different high pressure devices were used at the Laboratoire Magmas et Volcans (Clermont-Ferrand, France) depending on the required experimental pressure: a single stage 1.91 cm (¾ in.) bore diameter piston cylinder, an end-load 1.27 cm (½ in.) bore diameter piston cylinder, and a Walker type multi-anvil. For the piston cylinder experiments, the assemblies were composed of outer salt and pyrex sleeves, a straight graphite furnace, and inner cylinders of crushable magnesia. The ¾-in. assembly had an additional pyrex sleeve between graphite furnace and the crushable MgO. The multi-anvil assembly consisted of a natural pyrophyllite gasket in combination with prefabricated Cr-doped MgO-octahedral, a zirconium isolation sleeve, a stepped graphite furnace, and inner crushable MgO parts. Further experimental details are discussed in Vielzeuf and Montel (1994) and Auzanneau et al. (2006). In this type of experiment, which have minute subsolidus fluid content and are fluid-undersaturated at supersolidus conditions, oxygen fugacity cannot be controlled by conventional double capsule buffer techniques. However, the presence and nature of the iron-bearing phases indicate that, with respect to the starting materials, no drastic change in oxygen fugacity took place during the experiments.

Attainment of equilibrium

Textural equilibration, homogeneous distribution of all phases over the capsules (Fig. 1), homogeneous composition of phases in the charges, and consistency between different experiments show that most experimental products are at or close to equilibrium. Nevertheless, relict Fe-rich cores persist on garnet grains that were present in the pelitic starting material. In a few experiments, newly crystallized phases (garnet in the greywacke and clinopyroxene in both samples) are zoned. This compositional zoning is probably due to disequilibrium crystallization of a core at the beginning of the experiment. For this study, we assume that the rim of zoned grains is in equilibrium with the remaining phases.

Phase analyses

Analyses were carried out with a Cameca SX100 electron microprobe at the Université Blaise Pascal (Clermont-Ferrand, France) and a Jeol JXA8200 electron microprobe

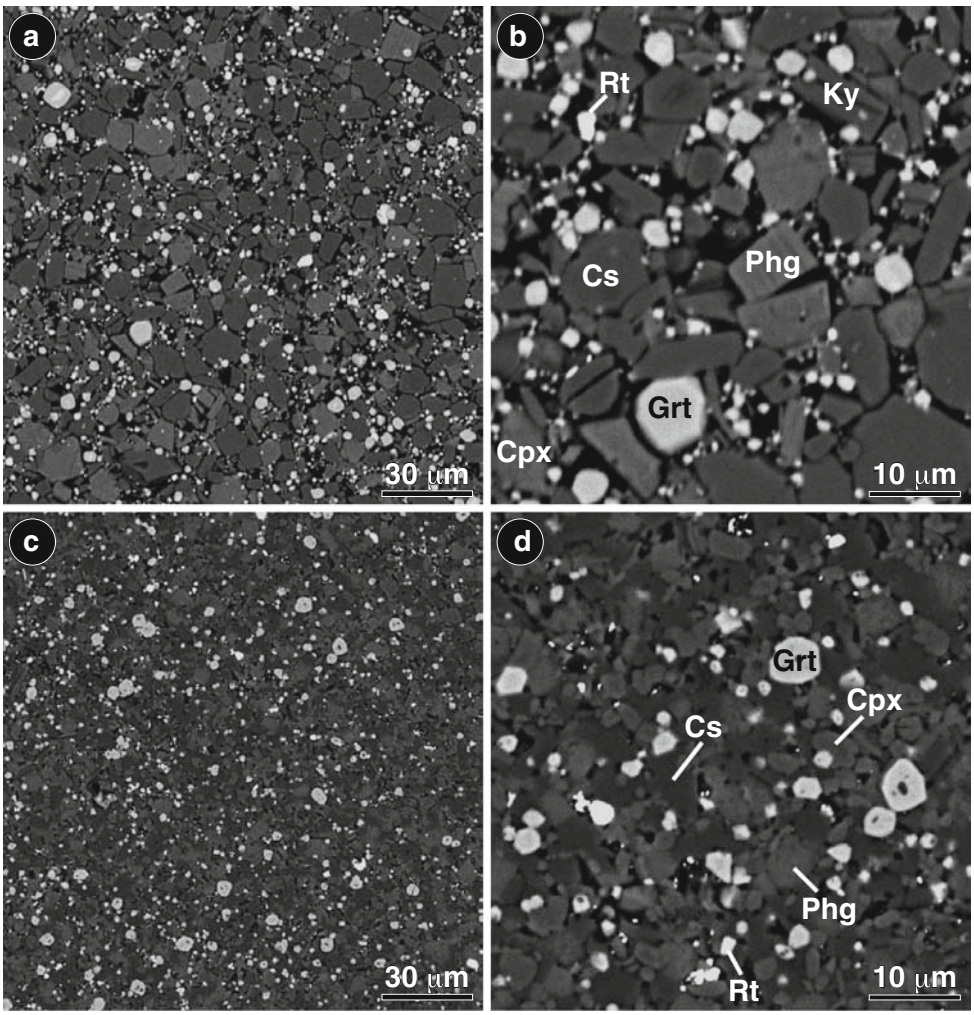

Fig. 1 BSE images of two experiments performed from the pelitic sample CO at 900°C—6.0 GPa (**a**, **b**) and from the greywacke CEVP at 900°C—5.0 GPa (**c**, **d**). Note the coexistence of rutile, phengite and coesite and the homogenous distribution of phases over the images attesting the equilibration of the samples during the experiments

at the Institut for Mineralogy and Petrology of ETH (Zurich, Switzerland). Operating conditions were 15 kV accelerating voltage and 15 nA sample current. Oxide and silicate standards were used for calibration. Counting times were 10 s on the peak and 5 s on the background, measured before and after the peak. Four spectrometers were used simultaneously with Na and K analyzed first to minimize losses. A ZAF correction procedure was applied. In most experimental products, grain sizes are small (<5 μm). To avoid contamination by surrounding phases, the electron beam was focused to the minimum size ($d < 100$ nm). For phengite, comparative analyses have been performed employing a beam current of 15 and 10 nA. No change in K_2O content has been noted indicating that no significant K_2O loss happened during analysis under the 15 nA beam. The best analyses of phengite were selected considering the following criteria: no CaO, sum of cations in the interlayer site close to 1 (normalization on the basis of 11 oxygen atoms), sum of cations in octahedral sites close to 2 (or slightly higher). The presence of rutile grains in the matrix and the possible TiKα secondary fluorescence in such grains induced by FeKα primary fluorescence emitted by Fe-bearing phases during analysis can cause an overestimate of phengite TiO_2 concentration. To avoid the effect of secondary fluorescence, we have not only analysed phengite grains in the neighbourhood of rutile grains, but also analysed phengites surrounded by quartz/coesite or kyanite.

Phengite structural formula calculations

The electron microprobe analyses do not quantify hydrogen and ferrous/ferric iron ratio. Thus, some assumptions must be made to calculate structural formulae. In natural muscovite, analyses show that even at low oxygen fugacities, the proportion of ferric iron is important and represents 50–60% of the total iron (Guidotti and Sassi 1998a; Schmid et al. 2003). When ferric iron is disallowed during structural formula calculation, the Fe^{2+} content and the Fe^{2+}/Mg ratio are overestimated (Guidotti et al. 1994; Guidotti and Sassi 2002). This can have significant effects on thermodynamic calculations. Moreover, although mica

can be deficient in H (Dyar et al. 1993), this deficit is considered as minor and negligible. Consequently, the analyses are normalized to 11 oxygen atoms ($10O^{2-}$ + $2OH^{-}$ per formula unit) and Fe^{3+} is in a first approximation set to 50% of the total iron.

Experimental results

Phase assemblages

Phengite + rutile is present in 48 experiments ranging from 1.5 to 8.0 GPa, and from 790 to 1,050°C, 30 experiments being from the metagreywacke and 18 from the metapelite (Table 2). Silicate melt was observed in 7 experiments performed on the pelite and 16 performed on the greywacke. The solidus has a positive slope for both lithologies. In the case of the greywacke, melt appears at about 800°C at 2.5 GPa; 850°C at 3.8 GPa and 900°C at 5.2 GPa (Auzanneau et al. 2006). The solidus of the pelite is slightly shifted towards lower temperatures (Schmidt et al. 2004). In most experiments, phengite coexists with an eclogitic assemblage: garnet + jadeite/omphacite + quartz/coesite ± kyanite ± melt. At low temperature and low pressure ($T \leq 850$°C and $P \leq 2.5$ GPa), plagioclase (±K-feldspar) and biotite are stable and omphacite is not always present. In this *P–T* domain, phengite coexists with garnet ± omphacite ± plagioclase + biotite + quartz + melt ± kyanite. In all run products reported in this study rutile is present, indicating TiO_2-saturation.

Phase compositions

The average phase compositions are given in the electronic appendix.

Biotite is present in 9 experiments performed between 1.5 and 2.4 GPa and 800–850°C and has been analysed in 6 of them. The biotite compositions from the pelite and the greywacke are similar, except for Al which is slightly higher in the kyanite-saturated pelite. Biotites are Mg-rich and $X_{\text{Fe-total}}$ ranges from 0.24 to 0.45. Their compositions are characterised by high Si-content (Si = 2.8–3.0) and moderate cation deficiency in the interlayer site (average $\sum \text{cat}^{\text{XII}} = 0.94$) indicating that solid solution with talc observed by Hermann (2002) is moderate. Nevertheless, all biotites have an important cation deficiency in the octahedral sites (average $\sum \text{cat}^{\text{VI}} = 2.59$). This strong deviation from the ideal trioctahedral occupancy has been observed by Robert (1976) and Massonne and Schreyer (1987). It is interpreted as an incorporation of a dioctahedral component at high pressure approaching the upper stability limit (Guidotti 1984; Patiño Douce and McCarthy 1998). Nevertheless, such low octahedral occupancies are not common in natural metamorphic biotite and deviation towards dioctahedral mica is not well documented and understood. As observed by Guidotti et al. (1977), biotite is significantly richer in Ti than phengite and the partition coefficient $D_{\text{Ti}}^{\text{Phg/Bt}}$ ranges from 0.31 to 0.69.

Plagioclase is present in 6 experiments performed at low pressure and low temperature and K-feldspar coexists with plagioclase in two charges. Plagioclase is albite-rich ($X_{\text{Ab}} = 0.68$–0.81; $X_{\text{An}} = 0.14$–0.28; $X_{\text{Or}} = 0.04$–0.13). The orthoclase-content is the highest ($X_{\text{Or}} > 0.10$) in two experiments were plagioclase coexists with K-feldspar. For these two experiments, the temperature of equilibrium calculated from coexisting feldspar pairs is in good agreement with the experimental conditions (PC3-2001-1_{CEVP}: $P_{\text{exp}} = 2.3$ GPa, $T_{\text{exp}} = 850$°C, $T_{\text{calc}} = 875 \pm 32$°C; PC3-2002-$1_{\text{CO}}$: $P_{\text{exp}} = 1.8$ GPa, $T_{\text{exp}} = 850$°C, $T_{\text{calc}} = 875 \pm 17$°C; Lindsley and Nekvasil 1989) demonstrating that thermodynamic equilibrium was reached during the experiment. As these experiments are at the low pressure, low-temperature end of our experimental range, it can be deduced, that the other experiments reached equilibrium as well.

Garnet is present in all experimental products. For both starting materials, garnet is devoid of majoritic component, even at the highest pressures. The garnet composition changes drastically with pressure, temperature and coexisting assemblage (pelite: $X_{\text{Alm}} = 0.53 \rightarrow 0.65$; $X_{\text{Py}} = 0.20 \rightarrow 0.31$; $X_{\text{Grs}} = 0.08 \rightarrow 0.21$; $X_{\text{Fe}} = 0.63 \rightarrow 0.76$—greywacke: $X_{\text{Alm}} = 0.49 \rightarrow 0.69$; $X_{\text{Py}} = 0.18 \rightarrow 0.36$; $X_{\text{Grs}} = 0.09 \rightarrow 0.28$; $X_{\text{Fe}} = 0.58 \rightarrow 0.79$). Minor quantities of Mn, Ti and Na are also present in garnet. The Ti and Na contents vary with pressure in a similar fashion (Fig. 2a, b) indicating that the coupled substitution $(Na^{+})^{\text{VIII}} + (Ti^{4+})^{\text{VI}} = (R^{2+})^{\text{VIII}} + (Al^{3+})^{\text{VI}}$ described by Ringwoog and Lovering (1970) and Bishop et al. (1976, 1978) is a major substitution to balance Ti in garnet at these *P–T* conditions. At a given pressure and temperature, the Ti contents in the pelitic garnets are in general lower than those of the greywacke, especially around 4 GPa (TiO_2: pelite = 0.2 → 0.7 wt%; greywacke = 0.3 → 2.0 wt%) and the change of slope is less obvious. In both samples, garnet has a lower Ti content than phengite but the difference tends to decrease with increasing pressure. Thus, $D_{\text{Ti}}^{\text{Phg/Grt}}$ ranges over a large interval (pelite = 1.0–6.9; greywacke = 0.9–3.5) and tends to decrease with increasing pressure.

Clinopyroxene coexists with phengite in all experiments from the greywacke, except at 1.9 GPa 800°C. In the pelite, it is present in the pressure range 2.4–8.0 GPa. In both samples, the clinopyroxene is a jadeite-rich omphacite. Diopside-hedenbergite, clinoenstatite-clinoferrosilite and Ca-eskolaite are major components while Ca-Tschermak and $CaTiAl_2O_6$ remain minor (normalization after Cawthorn

Table 2 Experimental results

Run *n*°	*P* (GPa)	*T* (°C)	*t* (h)		Phases present
Metagreywacke CEVP					
PC3-2001-13	1.9	800	228	PC½	Qz, Pl, Bt, Phg, Grt, Rt, Glass[b, e]
PC3-2001-12	2.1	800	228	PC½	Qz, Pl, Bt, Cpx, Phg, Grt, Rt, Glass[b,c]
PC3-2000-13B	2.3	850	256	PC½	Qz, Pl, Bt, Grt, Phg, Cpx, Rt, Glass[b,c]
PC3-2001-1	2.3	850	198	PC½	Qz, Pl, K-Fs, Bt, Grt, Phg, Cpx, Rt, Glass[b,c]
PC3-2000-5	2.4	800	238	PC½	Qz, Cpx, Phg, Grt, Rt, Glass, (Bt)[b,c]
PC3-2000-8	2.4	850	162	PC½	Qz, Cpx, Phg, Grt, Rt, Glass, (Bt)[b,c]
PC3-2001-16	2.4	850	181	PC½	Qz, Cpx, Phg, Grt, Rt, Glass, (Bt)[b,c]
PC3-2001-11	2.4	870	164	PC½	Qz, Cpx, Phg, Grt, Rt, Glass[b,c]
PC3-2000-10	2.4	900	140	PC½	Qz, Cpx, Phg, Grt, Rt, Glass[b,c]
PC3-2000-7	2.8	800	159	PC½	Qz, Cpx, Phg, Grt, Rt[b,e]
PC3-2000-12	2.8	900	136	PC½	Qz, Cpx, Phg, Grt, Rt, Glass[b,e]
PC3-2000-3	2.8	950	48	PC½	Qz, Cpx, Phg, Grt, Rt, Glass[d,e]
PC3-2001-10	3.3	900	169	PC½	Cs, Cpx, Phg, Grt, Rt, Glass[d,e]
ME36	4.0	790	141	ME	Cs, Cpx, Phg, Grt, Rt[a,e]
ME35	4.0	850	96	ME	Cs, Cpx, Phg, Grt, Rt[a,e]
ME32	4.0	900	60	ME	Cs, Cpx, Phg, Grt, Rt, Glass[a,e]
ME40	4.0	950	122	ME	Cs, Cpx, Phg, Grt, Rt, Glass[a,e]
ME207	5.0	850	143	ME	Cs, Cpx, Phg, Grt, Rt[a,e]
ME142	5.0	900	162	ME	Cs, Cpx, Phg, Grt, Rt, Glass[b,e]
ME202	5.0	900	59	ME	Cs, Cpx, Phg, Grt, Rt, Glass[a,e]
ME107	5.5	810	51	ME	Cs, Cpx, Phg, Grt, Rt[a,e]
ME208	6.0	850	168	ME	Cs, Cpx, Phg, Grt, Rt, (Carb)[d,e]
ME204	6.0	900	143	ME	Cs, Cpx, Phg, Grt, Rt[a,e]
ME219	6.0	900	124	ME	Cs, Cpx, Phg, Grt, Rt[d,e]
ME96	6.5	1050	71	ME	Cs, Cpx, Phg, Grt, Rt[a,e]
ME209	7.0	850	190	ME	Cs, Cpx, Phg, Grt, Rt[d,e]
ME205	7.0	900	142	ME	Cs, Cpx, Phg, Grt, Rt[d,e]
ME106	7.5	910	45	ME	Cs, Cpx, Phg. Grt, Rt[a,e]
ME237	8.0	850	211	ME	Cs, Cpx, Phg, Grt, Rt, (Law)[d,e]
ME211	8.0	900	214	ME	Cs, Cpx, Phg, Grt, Rt[d,e]
Metapelite CO					
PC2-2002-26	1.5	800	211	PC3/4	Qz, Ky, Pl, Bt, Phg, Grt, Rt, Glass[d,e]
PC3-2002-1	1.8	850	351	PC½	Qz, Ky, Pl, K-Fs, Bt, Phg, Grt, Rt, Glass[d,e]
PC3-2002-6	2.4	900	207	PC½	Qz, Ky, Cpx, Phg, Grt, Rt, Glass[d,e]
ME36	4.0	790	141	ME	Cs, Ky, Cpx, Phg, Grt, Rt[a,e]
ME35	4.0	850	96	ME	Cs, Ky, Cpx, Phg, Grt, Rt, Glass[a,e]
ME32	4.0	900	60	ME	Cs, Ky, Cpx, Phg, Grt, Rt, Glass[a,e]
ME40	4.0	950	122	ME	Cs, Ky, Cpx, Phg, Grt, Rt, Glass[a,e]
ME207	5.0	850	143	ME	Cs, Ky, Cpx, Phg, Grt, Rt[a,e]
ME202	5.0	900	59	ME	Cs, Ky, Cpx, Phg, Grt, Rt, Glass[a,e]
ME107	5.5	810	51	ME	Cs, Ky, Cpx, Phg, Grt, Rt[a,e]
ME208	6.0	850	168	ME	Cs, Ky, Cpx, Phg, Grt, Rt, (Carb)[d,e]
ME219	6.0	900	124	ME	Cs, Ky, Cpx, Phg, Grt, Rt[a,e]
ME209	7.0	850	190	ME	Cs, Ky, Cpx, Phg, Grt, Rt[d,e]
ME205	7.0	900	142	ME	Cs, Ky, Cpx, Phg, Grt, Rt[d,e]
ME95	7.3	1000	75	ME	Cs, Ky, Cpx, Phg, Grt, Rt[a,e]
ME106	7.5	910	45	ME	Cs, Ky, Cpx, Phg. Grt, Rt[a,e]

Table 2 continued

Run $n°$	P (GPa)	T (°C)	t (h)		Phases present
ME237	8.0	850	211	ME	Cs, Ky, Cpx, Phg, Grt, Rt[d,e]
ME211	8.0	900	214	ME	Cs, Ky, Cpx, Phg, Grt, Rt[d,e]

Origin of data: a) Phase determination from Schmidt et al. (2004). b) Phase determination from Auzanneau et al. (2006). c) Phengite analysis from Auzanneau et al. (2006). d) Phase determination from this study. e) Phengite analysis from this study

PC1/2″ 1.27 cm piston cylinder, *PC3/4″* 1.91 cm piston cylinder, *ME* multi-anvil, *t* duration of the experiment measured from the attainment of desired *T* and *P* to the quench, *Bt* biotite, *Carb* carbonate, *Cs* coesite, *Cpx* clinopyroxene, *Grt* garnet, *K-Fs* alkali feldspar, *Ky* kyanite, *Law* lawsonite, *Phg* phengite, *Pl* plagioclase, *Qz* quartz, *Rt* rutile. Other accessory phases observed in every run products from 1.5 to 8.0 GPa: monazite, apatite, iron sulfur, zircon, scheelite

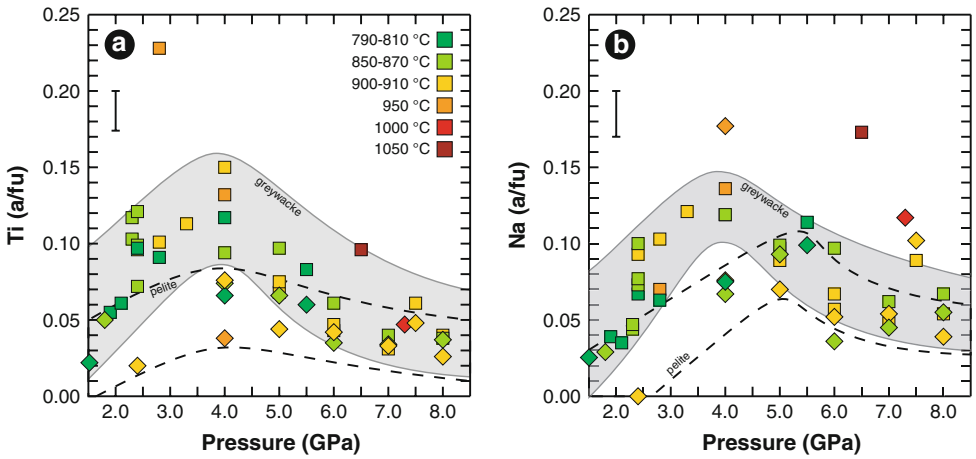

Fig. 2 The Ti (**a**) and Na (**b**) contents in garnet between 1.5 and 8.0 GPa (analyses normalized to 24 oxygens). The similar evolution of the two elements with pressure reveals the importance of the substitution $(Na^{+})^{VIII} + (Ti^{4+})^{VI} = (R^{2+})^{VIII} + (Al^{3+})^{VI}$ to balance Ti in garnet in this *P–T* domain. *Square* greywacke, *diamond* pelite

and Collerson 1974). The omphacites show important compositional changes with pressure, temperature and coexisting phases (pelite: $X_{Jd} = 0.57 \rightarrow 0.88$; $X_{Diop + Hd} = 0.04 \rightarrow 0.14$; $X_{Ens + Fs} = 0.01 \rightarrow 0.12$; $X_{Ca\text{-}Esko} = 0.04 \rightarrow 0.20$—greywacke: $X_{Jd} = 0.41 \rightarrow 0.84$; $X_{Diop + Hd} = 0.07 \rightarrow 0.39$; $X_{Ens + Fs} = 0.02 \rightarrow 0.20$; $X_{Ca\text{-}Esko} = 0.01 \rightarrow 0.14$). As observed in the case of phengite and garnet, Ti contents are sensitive to the crystallisation conditions: $CaTiAl_2O_6$ tends to increase with temperature and to decrease with pressure (Fig. 3). Clinopyroxenes always have a much lower Ti content than phengite (average values of $D_{Ti}^{Phg/Cpx}$: pelite = 4.7; greywacke = 4.4).

The silicate melts from some of the experiments performed between 2.3 and 5.0 GPa and 850 and 900°C were analyzed (greywacke: 5 analyses and pelite: 2 analyses). For both lithologies, the silicate melts are similar in composition and correspond to slightly peraluminous leucogranites. They are rich in SiO_2 (67–71 wt%), Al_2O_3 (12–15 wt%), Na_2O (2–5 wt%), K_2O (4–7 wt%) and H_2O (3–11 wt%, determined by mass balance calculations) and poor in FeO (0.5–1.1 wt%), MgO (<0.4 wt%), MnO (<0.1 wt%), CaO (<0.9 wt%) and TiO_2 (0.2–0.8 wt%). The composition

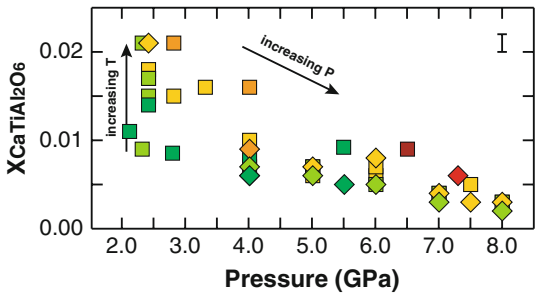

Fig. 3 Evolution of the molar fraction of the $CaTiAl_2O_6$ component in clinopyroxene between 2.1 and 8.0 GPa. *Square* greywacke, *diamond* pelite, *color legend* (see Fig. 2a)

of the silicate melt changes with pressure: SiO_2, Al_2O_3 and Na_2O tend to decrease while FeO, K_2O and H_2O increase with increasing pressure. Ti-contents of the melts increase weakly with both temperature and pressure.

Phengite compositions are reported in Table 3. At a given P–T condition, phengites crystallized from the two bulk compositions differ in composition. In the metagreywacke, they are richer in Si and Mg and poorer in Al^{IV} and Al^{VI} than in the Al_2SiO_5-saturated metapelite. These compositional

Table 3 Phengite compositions

Run $n°$	P (GPa)	T (°C)	SiO_2	TiO_2	Al_2O_3	FeO	MnO	MgO	CaO	Na_2O	K_2O	Total
Metagreywacke CEVP												
PC3-2001-13	1.9	800	49.16	1.43	28.49	2.92	0.00	2.86	0.04	0.79	9.83	95.52
SD (9)			1.30	0.08	0.48	0.21	0.01	0.22	0.01	0.06	0.24	
PC3-2001-12	2.1	800	50.85	1.28	27.17	2.86	0.00	3.17	0.02	0.96	9.22	95.52
SD (4)			1.19	0.06	1.16	0.09	0.01	0.13	0.02	0.04	0.38	
PC3-2000-13B	2.3	850	48.70	3.10	27.23	2.00	0.00	4.13	0.02	0.69	9.65	95.52
SD (2)			0.09	0.12	0.23	0.08	0.00	0.05	0.01	0.03	0.04	
PC3-2001-1	2.3	850	50.13	2.01	25.58	2.98	0.03	3.96	0.06	0.78	9.75	95.28
SD (6)			0.48	0.18	0.67	0.18	0.01	0.22	0.06	0.09	0.11	
PC3-2000-5	2.4	800	50.04	1.66	26.07	4.07	0.00	3.91	0.06	1.06	8.65	95.53
SD (5)			0.52	0.09	0.43	0.19	0.02	0.15	0.03	0.09	0.18	
PC3-2000-8	2.4	850	49.98	1.81	26.90	3.42	0.01	3.07	0.06	0.96	9.31	95.53
SD (2)			1.29	0.13	0.45	0.01	0.01	0.07	0.02	0.11	0.03	
PC3-2001-16	2.4	850	50.63	2.05	25.32	2.98	0.04	3.70	0.16	1.47	9.17	95.51
SD (4)			0.32	0.10	0.42	0.25	0.01	0.17	0.03	0.19	0.18	
PC3-2001-11	2.4	870	48.79	2.84	26.51	2.57	0.01	4.19	0.06	0.73	9.82	95.52
SD (6)			0.85	0.19	0.43	0.23	0.02	0.22	0.02	0.06	0.09	
PC3-2000-10	2.4	900	49.96	2.53	25.74	3.09	0.00	3.53	0.04	0.60	10.05	95.54
SD (3)			0.06	0.20	0.19	0.10	0.00	0.10	0.01	0.08	0.22	
PC3-2000-7	2.8	800	51.04	1.63	25.10	3.66	0.00	4.41	0.10	0.59	9.01	95.54
SD (2)			0.16	0.12	0.16	0.26	0.02	0.28	0.02	0.03	0.15	
PC3-2000-12	2.8	900	48.71	2.44	27.31	2.47	0.02	4.22	0.03	0.62	9.68	95.51
SD(2)			0.49	0.07	0.45	0.02	0.00	0.13	0.01	0.00	0.01	
PC3-2000-3	2.8	950	48.34	3.68	27.63	1.76	0.00	3.07	0.02	0.37	10.68	95.54
SD (2)			0.16	0.23	0.23	0.03	0.00	0.11	0.02	0.01	0.06	
PC3-2001-10	3.3	900	49.52	2.20	26.87	2.57	0.01	3.47	0.03	0.38	10.49	95.53
SD (2)			0.44	0.08	0.09	0.01	0.01	0.11	0.03	0.05	0.08	
ME36	4.0	790	50.64	1.31	24.46	2.12	0.01	3.85	0.01	0.18	10.53	93.11
SD (7)			0.30	0.03	0.29	0.11	0.01	0.09	0.01	0.04	0.22	
ME35	4.0	850	51.36	1.55	24.82	2.26	0.00	3.79	0.01	0.21	9.59	93.58
SD (5)			0.73	0.03	0.29	0.06	0.01	0.07	0.00	0.01	0.29	
ME32	4.0	900	53.49	2.33	26.74	2.16	0.02	3.64	0.05	0.36	10.89	99.66
SD (2)			1.18	0.04	0.53	0.01	0.02	0.01	0.01	0.04	0.06	
ME40	4.0	950	49.71	2.04	24.96	2.10	0.01	3.52	0.03	0.26	9.90	92.51
SD (12)			0.76	0.08	0.41	0.06	0.01	0.16	0.02	0.05	0.12	
ME207	5.0	850	51.74	0.96	25.17	2.45	0.01	4.22	0.01	0.25	10.71	95.52
SD (5)			0.29	0.07	0.48	0.06	0.01	0.21	0.01	0.05	0.05	
ME142	5.0	900	50.78	1.23	24.37	2.38	0.00	4.02	0.02	0.14	10.78	93.64
SD (6)			0.41	0.04	0.52	0.06	0.01	0.17	0.01	0.02	0.17	
ME202	5.0	900	51.00	1.37	24.53	2.58	0.03	3.73	0.03	0.19	10.72	94.17
SD (6)			0.36	0.04	0.43	0.06	0.01	0.08	0.02	0.01	0.18	
ME107	5.5	810	53.50	1.05	20.39	3.11	0.04	4.61	0.11	0.33	10.28	93.42
SD (4)			0.20	0.03	0.14	0.15	0.04	0.10	0.11	0.13	0.21	
ME208	6.0	850	52.04	0.58	25.21	2.21	0.00	4.51	0.03	0.07	10.87	95.51
SD (14)			0.41	0.05	0.34	0.14	0.01	0.17	0.02	0.02	0.25	
ME204	6.0	900	51.71	0.80	25.74	2.15	0.01	4.29	0.01	0.08	10.72	95.52
SD (5)			0.15	0.04	0.43	0.07	0.01	0.12	0.01	0.01	0.10	
ME219	6.0	900	51.96	0.85	25.17	2.39	0.00	4.21	0.02	0.09	10.82	95.52
SD (10)			0.41	0.04	0.44	0.17	0.01	0.18	0.03	0.03	0.30	

Table 3 continued

Run *n*°	*P* (GPa)	*T* (°C)	SiO_2	TiO_2	Al_2O_3	FeO	MnO	MgO	CaO	Na_2O	K_2O	Total
ME96	6.5	1050	50.45	1.92	23.45	2.49	0.04	3.66	0.03	0.08	10.65	92.78
SD (5)			0.35	0.04	0.24	0.12	0.03	0.07	0.01	0.03	0.20	
ME209	7.0	850	52.83	0.47	24.38	2.40	0.01	4.38	0.02	0.04	10.98	95.52
SD (6)			0.44	0.06	0.31	0.10	0.01	0.07	0.02	0.02	0.09	
ME205	7.0	900	52.75	0.61	23.76	2.25	0.01	4.93	0.01	0.06	11.14	95.51
SD (11)			0.55	0.09	0.33	0.08	0.01	0.18	0.01	0.01	0.15	
ME106	7.5	910	52.72	0.53	19.33	2.72	0.02	4.94	0.03	0.17	10.25	90.72
SD (3)			0.37	0.04	0.24	0.13	0.02	0.07	0.04	0.08	0.06	
ME237	8.0	850	55.81	0.31	19.83	2.75	0.00	5.78	0.05	0.01	11.00	95.53
SD (9)			0.48	0.03	0.25	0.05	0.01	0.10	0.01	0.02	0.14	
ME211	8.0	900	54.70	0.45	21.30	2.40	0.02	5.34	0.09	0.05	11.18	95.52
SD (10)			0.27	0.03	0.24	0.05	0.01	0.10	0.02	0.01	0.12	

Run *n*°	Si	Al^{IV}	Ti	Al^{VI}	Fe^{3+}	Fe^{2+}	Mg	ΣVI	K	Na	ΣXII	$X_{Fe^{2+}}$
Metagreywacke CEVP												
PC3-2001-13	3.274	0.726	0.072	1.510	0.081	0.081	0.284	2.028	0.835	0.101	0.936	0.223
SD (9)	0.037	0.037	0.004	0.016	0.006	0.006	0.019	0.013	0.022	0.008	0.023	0.016
PC3-2001-12	3.366	0.634	0.064	1.486	0.079	0.079	0.313	2.021	0.778	0.123	0.901	0.202
SD (4)	0.054	0.054	0.003	0.024	0.003	0.003	0.014	0.019	0.032	0.005	0.032	0.008
PC3-2000-13B	3.241	0.759	0.155	1.378	0.056	0.056	0.410	2.053	0.819	0.089	0.908	0.120
SD (2)	0.009	0.009	0.006	0.007	0.002	0.002	0.005	0.004	0.004	0.004	0.005	0.004
PC3-2001-1	3.352	0.648	0.101	1.368	0.083	0.083	0.395	2.031	0.832	0.102	0.934	0.174
SD (6)	0.027	0.027	0.009	0.021	0.005	0.005	0.021	0.016	0.012	0.012	0.018	0.010
PC3-2000-5	3.330	0.670	0.083	1.374	0.113	0.113	0.388	2.072	0.734	0.137	0.872	0.226
SD (5)	0.020	0.020	0.005	0.014	0.005	0.005	0.015	0.010	0.016	0.011	0.017	0.010
PC3-2000-8	3.327	0.673	0.091	1.437	0.095	0.095	0.304	2.022	0.791	0.124	0.915	0.238
SD (2)	0.036	0.036	0.006	0.012	0.002	0.002	0.008	0.010	0.014	0.015	0.018	0.004
PC3-2001-16	3.375	0.625	0.103	1.365	0.083	0.083	0.367	2.001	0.780	0.190	0.970	0.184
SD (4)	0.020	0.020	0.005	0.016	0.007	0.007	0.016	0.012	0.014	0.025	0.027	0.014
PC3-2001-11	3.260	0.740	0.143	1.348	0.072	0.072	0.417	2.052	0.837	0.094	0.931	0.147
SD (6)	0.028	0.028	0.009	0.017	0.006	0.006	0.020	0.013	0.011	0.008	0.014	0.013
PC3-2000-10	3.336	0.664	0.127	1.362	0.086	0.086	0.351	2.014	0.856	0.077	0.933	0.197
SD (3)	0.010	0.010	0.010	0.012	0.002	0.002	0.010	0.007	0.018	0.011	0.020	0.006
PC3-2000-7	3.390	0.610	0.081	1.355	0.102	0.102	0.436	2.076	0.764	0.076	0.839	0.189
SD (2)	0.012	0.012	0.006	0.017	0.007	0.007	0.026	0.013	0.012	0.003	0.012	0.014
PC3-2000-12	3.247	0.753	0.122	1.392	0.069	0.069	0.420	2.072	0.823	0.081	0.904	0.141
SD (2)	0.021	0.021	0.003	0.011	0.001	0.001	0.012	0.008	0.006	0.001	0.006	0.004
PC3-2000-3	3.230	0.770	0.185	1.406	0.049	0.049	0.305	1.994	0.910	0.048	0.958	0.138
SD (2)	0.010	0.010	0.010	0.012	0.001	0.001	0.010	0.006	0.006	0.001	0.006	0.004
PC3-2001-10	3.306	0.694	0.110	1.420	0.072	0.072	0.345	2.019	0.893	0.049	0.942	0.172
SD (2)	0.013	0.013	0.004	0.007	0.001	0.001	0.011	0.006	0.008	0.006	0.010	0.005
ME36	3.452	0.548	0.067	1.418	0.061	0.061	0.391	1.998	0.916	0.024	0.940	0.134
SD (7)	0.013	0.013	0.002	0.009	0.003	0.003	0.009	0.008	0.018	0.006	0.019	0.006
ME35	3.461	0.539	0.078	1.432	0.064	0.064	0.380	2.018	0.825	0.027	0.852	0.143
SD (5)	0.018	0.018	0.002	0.009	0.002	0.002	0.007	0.009	0.026	0.002	0.026	0.004
ME32	3.406	0.594	0.112	1.414	0.057	0.057	0.345	1.985	0.885	0.044	0.929	0.143
SD (2)	0.035	0.035	0.002	0.011	0.001	0.001	0.005	0.010	0.013	0.005	0.014	0.001
ME40	3.404	0.596	0.105	1.419	0.060	0.060	0.359	2.004	0.865	0.034	0.899	0.143
SD (12)	0.022	0.022	0.005	0.013	0.002	0.002	0.015	0.010	0.012	0.007	0.014	0.006

Table 3 continued

Run *n*°	Si	Al^{IV}	Ti	Al^{VI}	Fe^{3+}	Fe^{2+}	Mg	ΣVI	K	Na	ΣXII	$X_{Fe^{2+}}$
ME207	3.442	0.558	0.048	1.416	0.068	0.068	0.418	2.018	0.909	0.032	0.941	0.140
SD (5)	0.018	0.018	0.003	0.014	0.002	0.002	0.019	0.009	0.006	0.007	0.009	0.006
ME142	3.448	0.552	0.063	1.399	0.068	0.068	0.407	2.004	0.934	0.019	0.953	0.142
SD (6)	0.022	0.022	0.002	0.014	0.002	0.002	0.016	0.011	0.016	0.003	0.016	0.006
ME202	3.448	0.552	0.070	1.402	0.073	0.073	0.376	1.994	0.925	0.025	0.949	0.163
SD (6)	0.018	0.018	0.002	0.010	0.002	0.002	0.008	0.008	0.016	0.002	0.016	0.004
ME107	3.641	0.359	0.054	1.277	0.089	0.089	0.468	1.975	0.893	0.044	0.936	0.159
SD (4)	0.009	0.009	0.002	0.009	0.004	0.004	0.010	0.009	0.018	0.018	0.022	0.007
ME208	3.458	0.542	0.029	1.432	0.061	0.061	0.447	2.030	0.922	0.009	0.931	0.121
SD (14)	0.017	0.017	0.002	0.013	0.003	0.003	0.016	0.010	0.021	0.002	0.021	0.006
ME204	3.433	0.567	0.040	1.447	0.060	0.060	0.425	2.031	0.908	0.010	0.918	0.123
SD (5)	0.016	0.016	0.002	0.011	0.002	0.002	0.011	0.007	0.009	0.002	0.009	0.004
ME219	3.454	0.546	0.042	1.427	0.067	0.067	0.417	2.019	0.918	0.012	0.929	0.138
SD (10)	0.019	0.019	0.022	0.023	0.005	0.005	0.004	0.012	0.007	0.040	0.039	0.008
ME96	3.465	0.535	0.099	1.362	0.072	0.072	0.375	1.980	0.933	0.010	0.943	0.160
SD (5)	0.013	0.013	0.002	0.009	0.003	0.003	0.007	0.007	0.017	0.004	0.018	0.007
ME209	3.510	0.490	0.024	1.419	0.067	0.067	0.434	2.010	0.931	0.005	0.936	0.133
SD (6)	0.014	0.014	0.003	0.008	0.003	0.003	0.008	0.006	0.009	0.003	0.010	0.005
ME205	3.511	0.489	0.030	1.374	0.063	0.063	0.489	2.019	0.946	0.007	0.953	0.113
SD (11)	0.018	0.018	0.005	0.014	0.002	0.002	0.018	0.009	0.013	0.002	0.014	0.005
ME106	3.686	0.314	0.028	1.279	0.080	0.080	0.515	1.981	0.915	0.023	0.938	0.134
SD (3)	0.014	0.014	0.002	0.007	0.004	0.004	0.007	0.006	0.006	0.011	0.012	0.006
ME237	3.706	0.294	0.015	1.258	0.076	0.076	0.572	1.998	0.932	0.001	0.933	0.118
SD (9)	0.014	0.014	0.002	0.008	0.001	0.001	0.010	0.007	0.012	0.002	0.013	0.002
ME211	3.638	0.362	0.022	1.308	0.067	0.067	0.530	1.993	0.948	0.007	0.955	0.112
SD (10)	0.011	0.011	0.001	0.008	0.001	0.001	0.010	0.006	0.010	0.002	0.010	0.003

Run *n*°	*P* (GPa)	*T* (°C)	SiO_2	TiO_2	Al_2O_3	FeO	MnO	MgO	CaO	Na_2O	K_2O	Total
Metapelite CO												
PC-2002-26	1.5	800	48.57	1.32	30.37	2.47	0.01	2.02	0.09	0.86	9.06	94.76
SD (4)			0.69	0.11	0.55	0.52	0.01	0.38	0.09	0.08	0.18	
PC3-2002-1	1.8	850	48.63	2.34	28.04	2.61	0.03	3.08	0.10	0.87	9.81	95.52
SD (6)			0.86	0.05	0.79	0.06	0.01	0.13	0.02	0.08	0.16	
PC3-2002-6	2.4	900	49.21	2.70	27.95	2.51	0.00	2.88	0.12	0.61	9.79	95.88
SD (3)			0.69	0.06	0.61	0.10	0.01	0.09	0.03	0.06	0.16	
ME36	4.0	790	50.37	0.94	27.45	1.73	0.03	3.14	0.03	0.43	10.26	94.38
SD (6)			0.79	0.05	0.32	0.05	0.04	0.09	0.03	0.11	0.13	
ME35	4.0	850	49.73	1.21	27.48	1.56	0.02	3.09	0.03	0.48	10.08	93.68
SD (15)			0.51	0.11	0.35	0.14	0.02	0.11	0.03	0.14	0.14	
ME32	4.0	900	49.22	2.04	27.05	1.94	0.02	3.00	0.03	0.37	10.05	95.06
SD (3)			0.78	0.01	0.29	0.06	0.03	0.05	0.03	0.05	0.09	
ME40	4.0	950	49.89	1.69	27.04	2.07	0.03	2.82	0.04	0.88	9.92	94.37
SD (3)			0.56	0.03	0.45	0.06	0.04	0.05	0.04	0.13	0.19	
ME207	5.0	850	50.24	1.02	28.21	1.92	0.00	3.17	0.02	0.30	10.63	95.51
SD (2)			0.11	0.17	0.23	0.02	0.00	0.09	0.00	0.02	0.04	
ME202	5.0	900	49.85	1.17	27.90	2.32	0.02	3.35	0.03	0.22	10.66	95.52
SD (4)			0.30	0.07	0.11	0.09	0.02	0.05	0.03	0.01	0.06	
ME107	5.5	810	51.46	0.62	23.64	2.04	0.05	3.81	0.11	0.30	10.00	92.03

Table 3 continued

Run $n°$	P (GPa)	T (°C)	SiO_2	TiO_2	Al_2O_3	FeO	MnO	MgO	CaO	Na_2O	K_2O	Total
SD (5)			1.16	0.05	0.69	0.08	0.04	0.09	0.02	0.11	0.13	
ME208	6.0	850	52.37	0.63	26.22	2.34	0.03	3.96	0.04	0.08	10.68	96.36
SD (4)			0.37	0.01	0.37	0.22	0.02	0.14	0.03	0.02	0.28	
ME219	6.0	900	51.65	1.02	25.97	2.29	0.02	3.85	0.06	0.09	10.59	95.53
SD (5)			0.34	0.07	0.11	0.08	0.01	0.24	0.02	0.02	0.17	
ME209	7.0	850	52.83	0.46	24.42	2.40	0.01	4.36	0.02	0.04	10.96	95.52
SD (5)			0.33	0.06	0.25	0.12	0.01	0.08	0.02	0.02	0.10	
ME205	7.0	900	52.49	0.61	24.15	2.61	0.01	4.47	0.01	0.05	11.13	95.52
SD (6)			0.21	0.05	0.15	0.10	0.01	0.07	0.01	0.02	0.16	
ME95	7.3	1000	52.76	1.03	20.80	4.72	0.06	4.43	0.03	0.06	10.31	94.20
SD (5)			0.69	0.03	0.32	0.42	0.05	0.09	0.03	0.05	0.17	
ME106	7.5	910	54.16	0.59	21.30	2.78	0.02	4.61	0.01	0.17	10.63	94.27
SD (3)			0.08	0.05	0.28	0.10	0.02	0.13	0.01	0.04	0.09	
ME237	8.0	850	55.87	0.33	20.97	2.63	0.00	5.38	0.03	0.02	10.22	95.44
SD (8)			0.55	0.03	0.20	0.16	0.01	0.12	0.01	0.02	0.19	
ME211	8.0	900	54.48	0.44	21.92	2.71	0.04	5.18	0.03	0.03	10.71	95.53
SD (7)			0.29	0.03	0.14	0.06	0.01	0.12	0.02	0.02	0.18	

Run $n°$	Si	Al^{IV}	Ti	Al^{VI}	Fe^{3+}	Fe^{2+}	Mg	ΣVI	K	Na	ΣXII	$X_{Fe^{2+}}$
Metapelite CO												
PC-2002-26	3.238	0.762	0.066	1.623	0.069	0.069	0.201	2.028	0.770	0.112	0.882	0.255
SD (4)	0.029	0.029	0.005	0.030	0.015	0.015	0.037	0.020	0.016	0.010	0.019	0.054
PC3-2002-1	3.246	0.754	0.118	1.452	0.073	0.073	0.307	2.022	0.836	0.113	0.949	0.192
SD (6)	0.035	0.035	0.003	0.018	0.002	0.002	0.012	0.014	0.017	0.010	0.020	0.007
PC3-2002-6	3.268	0.732	0.135	1.456	0.070	0.070	0.285	2.015	0.830	0.078	0.908	0.196
SD (3)	0.026	0.026	0.003	0.014	0.003	0.003	0.009	0.010	0.016	0.008	0.017	0.008
ME36	3.376	0.624	0.047	1.544	0.049	0.049	0.313	2.002	0.877	0.056	0.933	0.134
SD (6)	0.023	0.023	0.003	0.008	0.001	0.001	0.010	0.009	0.013	0.015	0.017	0.005
ME35	3.356	0.644	0.061	1.542	0.044	0.044	0.311	2.002	0.868	0.063	0.930	0.124
SD (15)	0.021	0.021	0.005	0.011	0.004	0.004	0.011	0.010	0.012	0.018	0.019	0.010
ME32	3.330	0.670	0.104	1.487	0.055	0.055	0.302	2.003	0.867	0.049	0.916	0.154
SD (3)	0.023	0.023	0.001	0.007	0.002	0.002	0.006	0.007	0.011	0.006	0.012	0.004
ME40	3.353	0.647	0.085	1.495	0.058	0.058	0.282	1.979	0.851	0.115	0.966	0.171
SD (3)	0.020	0.020	0.002	0.011	0.002	0.002	0.005	0.009	0.018	0.016	0.022	0.005
ME207	3.335	0.665	0.051	1.543	0.053	0.053	0.314	2.014	0.901	0.039	0.939	0.145
SD (2)	0.010	0.010	0.009	0.010	0.001	0.001	0.009	0.005	0.004	0.003	0.005	0.004
ME202	3.319	0.681	0.059	1.508	0.065	0.065	0.332	2.028	0.905	0.028	0.934	0.163
SD (4)	0.009	0.009	0.004	0.006	0.003	0.003	0.005	0.003	0.007	0.001	0.007	0.006
ME107	3.535	0.465	0.032	1.449	0.058	0.058	0.390	1.988	0.877	0.040	0.917	0.130
SD (5)	0.037	0.037	0.002	0.017	0.002	0.002	0.010	0.014	0.017	0.014	0.020	0.005
ME208	3.443	0.557	0.031	1.476	0.064	0.064	0.388	2.024	0.896	0.011	0.907	0.142
SD (4)	0.017	0.017	0.000	0.013	0.006	0.006	0.013	0.011	0.022	0.002	0.022	0.012
ME219	3.429	0.571	0.051	1.460	0.064	0.064	0.381	2.019	0.897	0.012	0.909	0.143
SD (5)	0.011	0.011	0.003	0.013	0.002	0.002	0.023	0.012	0.015	0.002	0.015	0.008
ME209	3.510	0.490	0.023	1.422	0.067	0.067	0.432	2.011	0.929	0.006	0.934	0.134
SD (5)	0.012	0.012	0.003	0.008	0.003	0.003	0.009	0.006	0.010	0.003	0.010	0.005
ME205	3.497	0.503	0.031	1.393	0.073	0.073	0.444	2.012	0.946	0.006	0.952	0.141
SD (6)	0.008	0.008	0.002	0.007	0.003	0.003	0.007	0.006	0.013	0.003	0.013	0.005

Table 3 continued

Run *n*°	Si	Al^{IV}	Ti	Al^{VI}	Fe^{3+}	Fe^{2+}	Mg	ΣVI	K	Na	ΣXII	$X_{Fe^{2+}}$
ME95	3.582	0.418	0.053	1.246	0.134	0.134	0.449	2.016	0.893	0.008	0.901	0.230
SD (5)	0.022	0.022	0.002	0.016	0.011	0.011	0.010	0.011	0.015	0.006	0.016	0.016
ME106	3.642	0.358	0.030	1.330	0.078	0.078	0.462	1.978	0.912	0.022	0.933	0.145
SD (3)	0.011	0.011	0.002	0.009	0.003	0.003	0.013	0.007	0.007	0.005	0.009	0.006
ME237	3.689	0.311	0.016	1.321	0.073	0.073	0.529	2.011	0.861	0.003	0.863	0.121
SD (8)	0.014	0.014	0.001	0.009	0.004	0.004	0.012	0.008	0.015	0.002	0.015	0.007
ME211	3.615	0.385	0.022	1.329	0.075	0.075	0.512	2.014	0.906	0.003	0.910	0.128
SD (7)	0.010	0.010	0.002	0.007	0.002	0.002	0.011	0.007	0.015	0.002	0.015	0.003

differences are less important in the pressure range 6.0–8.0 GPa. At a given pressure, for both bulk compositions, the concentrations of Ti increases with temperature. This enrichment is less significant for the highest pressures. No other systematic change in composition with temperature is observed. The effect of pressure is more drastic (Fig. 4) and the same compositional trends generally apply for both bulk compositions. For the greywacke (Fig. 4a), at 850–900°C, Si and Mg increase while Ti and Al^{IV} decrease with pressure. The Fe^{2+} concentration does not change, thus (Mg + Fe^{2+}) increases with pressure and $X_{Fe^{2+}}$ decreases. Because of the pressure sensitivity of the inverse Tschermak substitution ($Al^{VI} + Al^{IV} = R^{2+} + Si$) in the potassic white mica (Ernst 1963), a decrease of the Al^{VI} with increasing pressure is expected. However, Al^{VI} does not decrease with pressure up to 7.0 GPa, until the Ti concentrations in phengite become very low (i.e. <0.02–0.03 a/fu). At this point, Al^{VI} decreases drastically between 7.0 and 8.0 GPa. In this latter pressure range, the Si and Mg + Fe^{2+} enrichments are stronger. The data obtained at 950–1,050°C also follow these trends. At 800°C, Ti contents are low and the pressure effect is less significant than at higher temperature. Moreover, Na decreases with pressure, contrary to K. For the pelite (Fig. 4b), the compositional changes with pressure are similar except for Al^{VI}, which starts to decrease at a lower pressure (5 GPa) than in the greywacke (7 GPa). In both data series no significant variation of the sum of the cations ($\sum cat.^{VI} = 1.98–2.09$ and $\sum cat.^{XII} = 0.84–1.01$) with pressure or temperature or phengite composition is observed.

Discussion of substitution mechanisms in phengite and their *P*, *T* dependence

The deviations from ideal potassic white mica

The presence of Na, the alkali deficit ($\sum cat.^{XII} < 1.0$) and the cation excess in the octahedral sites ($\sum cat.^{VI} > 2.0$) indicate deviations from the ideal system $K(R^{2+}, R^{3+}, R^{4+})_2(Si,Al)_4O_{10}(OH)_2$. According to the reviews of Guidotti and Sassi (1998a, b) and Agard et al. (2001), the alkali deficiency can be related to the substitution of K by H_3O^+, H_2O, NH_4^+, or trace elements like Ba, Sr, Rb and Cs (not significant in our study), or can be due to a pyrophyllitic substitution ($K + Al^{IV} = \square^{XII} + Si$). Thus, at present there is no consensus on the origin of the alkali deficiency in phengites (Gouzu et al., 2005), nevertheless, following Agard et al. (2001) and Parra et al. (2002) we consider that the last substitution mechanism is robust. The small cation excess in the octahedral sites suggests a limited deviation toward trioctahedral mica (Guidotti 1984; Guidotti and Sassi 1998a, b). Alkali deficit and octahedral excess are thus respectively interpreted as pyrophyllite ($Al_2Si_4O_{10}(OH)_2$) and phlogopite ($KMg_3Si_3AlO_{10}(OH)_2$) components. In the investigated *P*–*T* domain, our results show that these deviations can be significant and remain uncorrelated with pressure or temperature. Na contents reach up to 0.19 a/fu in our phengites without reaching saturation in a sodic white mica (paragonite, $NaAl_2Si_3AlO_{10}(OH)_2$) and Na-contents decrease as pressure increases. This is in agreement with previous observation: natural phengites commonly show a strong inverse correlation between Na and Si (and Mg + Fe^{2+}). This evolution is related to the enlargement of the interlayer XII-coordinated site in response to the enrichment in Si. Thus, it becomes difficult for the potassic mica structure to accommodate the relatively smaller Na cation as pressure increases (Guidotti and Sassi 1998a, b).

The substitution of titanium in phengite

The compositional changes with pressure at 850–900°C are the most suited to determine the substitution mechanism of titanium in phengite. At pressures lower than 6.0–7.0 GPa, the absence of significant variations of Al^{VI}, the decrease of Ti and Al^{IV}, and the enrichment in Mg and Si with increasing pressure may seem consistent with the bulk substitution (A) $Mg + 2Si = Ti + 2Al^{IV}$. However, the pressure sensitivity of the inverse Tschermak substitution causes phengites to become progressively more Si-rich with pressure (Ernst 1963; Velde 1965). Thus, we suggest that

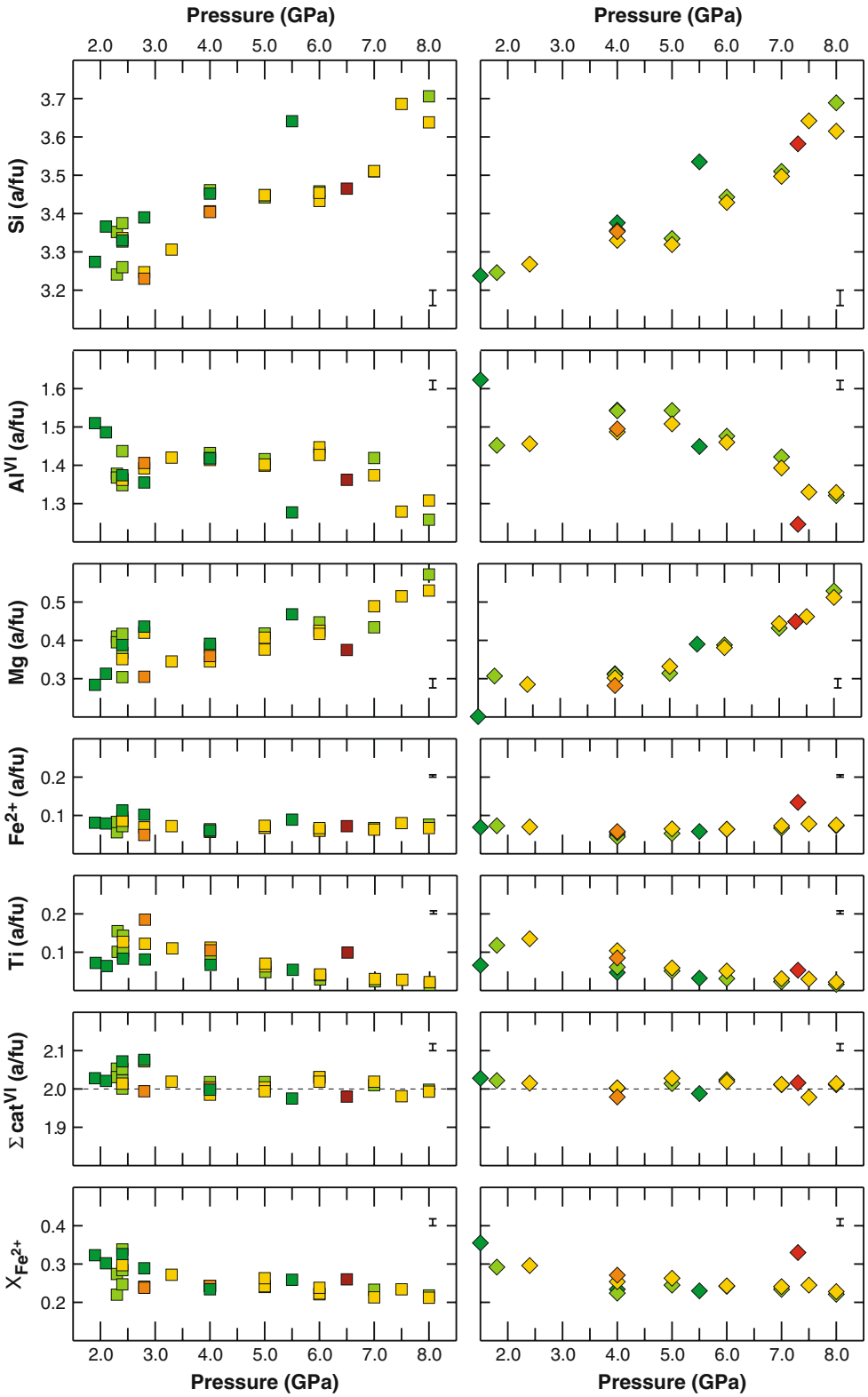

Fig. 4 Phengite compositions as a function of pressure at different temperatures. In spite of the difference in composition between the two starting materials, both data series have the same features, in particular the enrichment in Si and Mg, the decrease in Ti and the Al^{VI} plateau at pressure lower than 6.0–7.0 GPa. *Error bars* refer to standard deviations of analyses

the observed compositional variations with increasing pressure result from the combination of the classic Tschermak-substitution (B) $Si + Mg = AlP^{IVP} + AlP^{VIP}$ and either the substitution (C) $Al^{VI} + Si = Ti + Al^{IV}$ (with substitution A = B + C), or the substitution (D) $2Al^{VI} = Mg + Ti$ (with A = 2B + D). At pressures greater than 5–7 GPa, Ti-contents are < 0.05–0.03 Ti pfu and the importance of the substitution C or D becomes

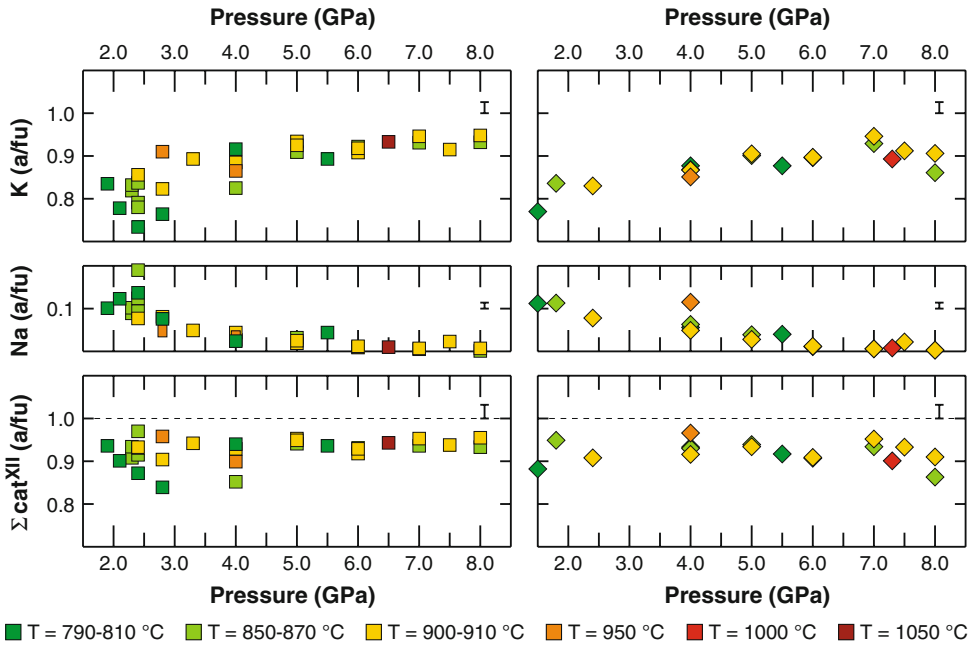

Fig. 4 continued

minor in comparison to the inverse Tschermak substitution and thus Al^{VI} decreases drastically. This interpretation requires further comments:

Because H_2O has not been analyzed, the identification of the major exchange vector for Ti could be distorted by the normalization procedure used to calculate the structural formula. For the biotite solid solution, it has been demonstrated that the Ti–oxy exchange ($R^{2+} + 2(OH)^- = Ti^{4+} + 2O^{2-} + H_2$) is a major substitution in Fe-rich biotite at high temperature (Dyar et al. 1993; Waters and Charnley 2002; Cesare et al. 2003; Henry et al. 2005). Our analysies does not entirely rule out this possibility. However, the Ti concentrations in our experimental phengites cover a wide interval (greywacke: 0.31–3.68 wt% TiO_2; pelite: 0.33–2.70 wt% TiO_2) and when analyses are normalised to a fixed number of cations ($\sum cat.^{VI+IV} = 6$; $\sum cat.^{XII} = 1$), the sum of cations charges ($\sum charge^{cat} =$ 21.8–22.1) does not vary systematically with temperature, pressure or composition. For these reasons, the Ti–oxy substitution is considered to be insignificant in our experimental charges.

Previously, only a few studies have considered substitution of Ti in potassic white micas and substitution D has been generally accepted as a substitution mechanism (Guidotti 1978; Tracy 1978; Zhang et al. 2002a, b; Hermann and Spandler 2008). However, no study provides irrefutable argumentation for the importance of the substitution at high pressure (Guidotti and Sassi 2002). Compared with the reference muscovite-aluminoceladonite join, both substitutions C and D lead to a deficit in Al with respect to Si. Thus, contrary to the suggestion of Hermann and Spandler (2008), the Al-deficit in Ti-rich phengite is not an indicator that Ti is incorporated by the substitution D. In addition, because the substitutions B, C and D are linearly dependent (C = B + D), the chosen substitutions have no consequence for describing and modelling the compositions. Thus, for a conventional mica model, the Ti-solution can be accounted for by introducing the Ti-phengite (TiP) endmember $KMgTiSi_3AlO_{10}(OH)_2$. In terms of mica substitution mechanisms and structural features, substitution C appears to be the most appropriate to explain the Ti decrease with pressure. Indeed, it is recognized that the inverse Tschermak substitution allows the enrichment in phengitic component (enrichment in Si) necessary to improve the fit between tetrahedral and octahedral sheets with increasing pressure (Ferraris and Ivaldi 2002). In a similar way, substitution C could allow the enrichment in phengitic component (i.e. in Si) as Ti decreases with increasing pressure, thus C is more suitable than D to explain the Ti decrease in Ti-rich phengite with pressure. Considering end-members, our data demonstrate that, as expected, the aluminoceladonite component (MgCel: $KMgAlSi_4O_{10}(OH)_2$) increases with pressure while the Ti-phengite component decreases with pressure (Fig. 5). It is thus not only a muscovite—celadonite but also the Ti-phengite—celadonite solid solution, which controls the Si content of phengites with pressure. The substitution mechanism for the Ti-enrichment with increasing temperature is probably different and remains to be explored.

Ti and Si as function of *P* and *T*

High Ti-concentrations and the correlation of Ti-content with temperature and the inverse of pressure are prominent

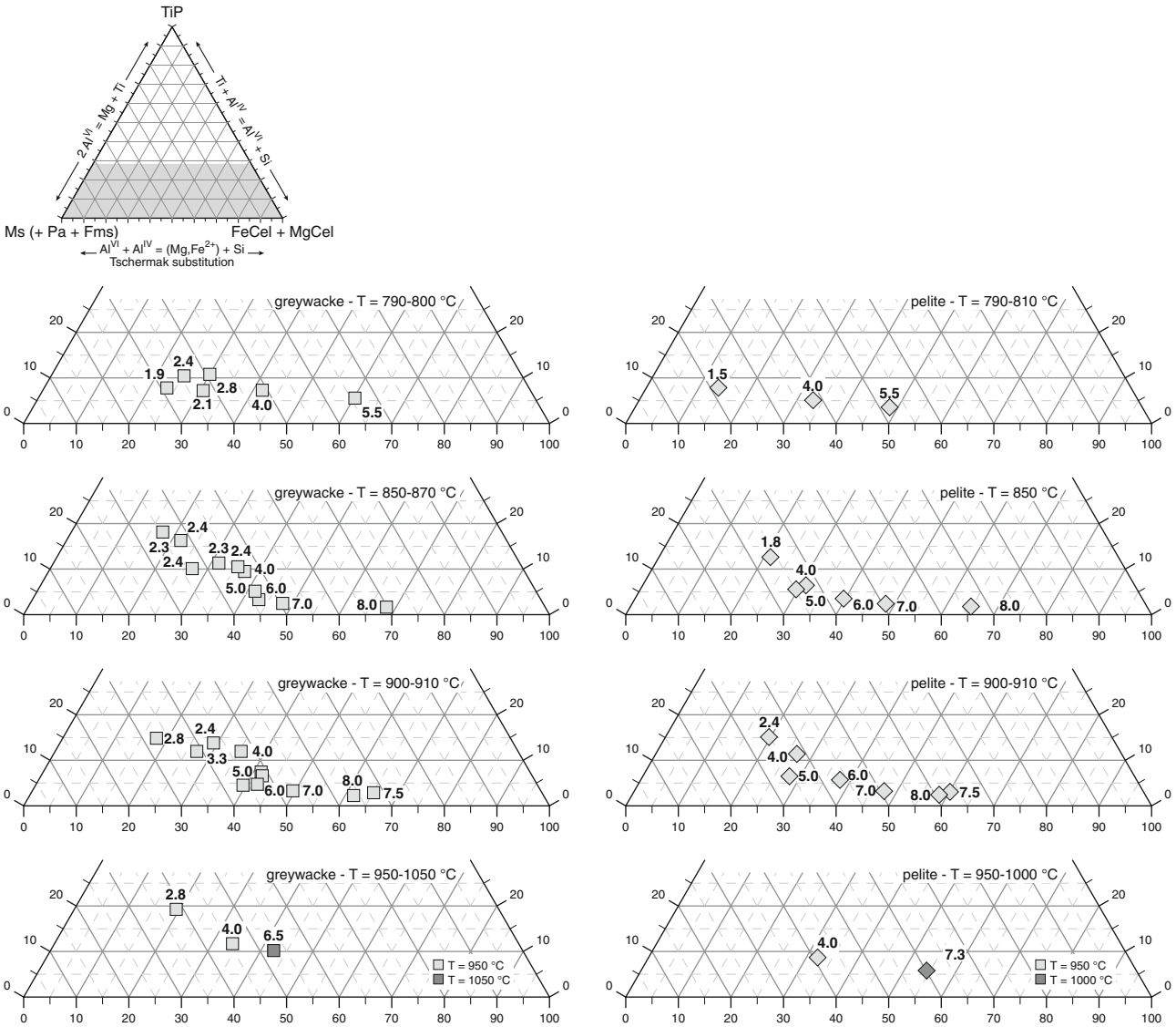

Fig. 5 Projection of phengite composition on the muscovite + paragonite + ferrimuscovite (Ms + Pa + Fms)—Ti-phengite (TiP)—Al-celadonite (MgCel + FeCel) plane

features in both series of experimental phengites (Fig. 6a, b). These results are reinforced by the composition of the experimental phengites of Hermann and Spandler (2008) from a rutile and quartz/coesite saturated pelite from 600 to 1,000°C, and from 2.5 to 4.5 GPa (circles in Fig. 6). Moreover, these characteristics are not specific to continental rocks as shown by the composition of experimental phengites produced at similar *P–T* condition from a basaltic rutile- and quartz/coesite-saturated eclogite (Schmidt et al. 2004; triangles in Fig. 6). The coherence between the four datasets confirms the behaviour of Ti over the investigated *T–P* space and shows that in rutile-quartz/coesite saturated rocks equilibrated at HT-(U)HP, the Ti content is significant and may have some effect on the Si content of phengites, in particular at higher temperatures. This is in part in agreement with the hypothesis of Guidotti and Sassi (1998a, b, 2002) stating that high Ti concentrations could be due to the combination of both high pressure and high temperature. More precisely, because of the negative correlation of Ti with pressure, the highest Ti contents in phengite are expected during decompression, when phengite progressively breaks down to form biotite in the stability field of rutile ($P > 2$ GPa in Al_2O_3 undersaturated rock—Auzanneau et al. 2006). As far as Si in phengite is concerned, even if the four datasets concern quartz/coesite-saturated bulk compositions, the Si data are not fully consistent (Fig. 6c). At a given *P–T* condition, the concentrations can be significantly different (even between the two pelites). Moreover, Si-contents show different correlations with pressure and do not systematically change

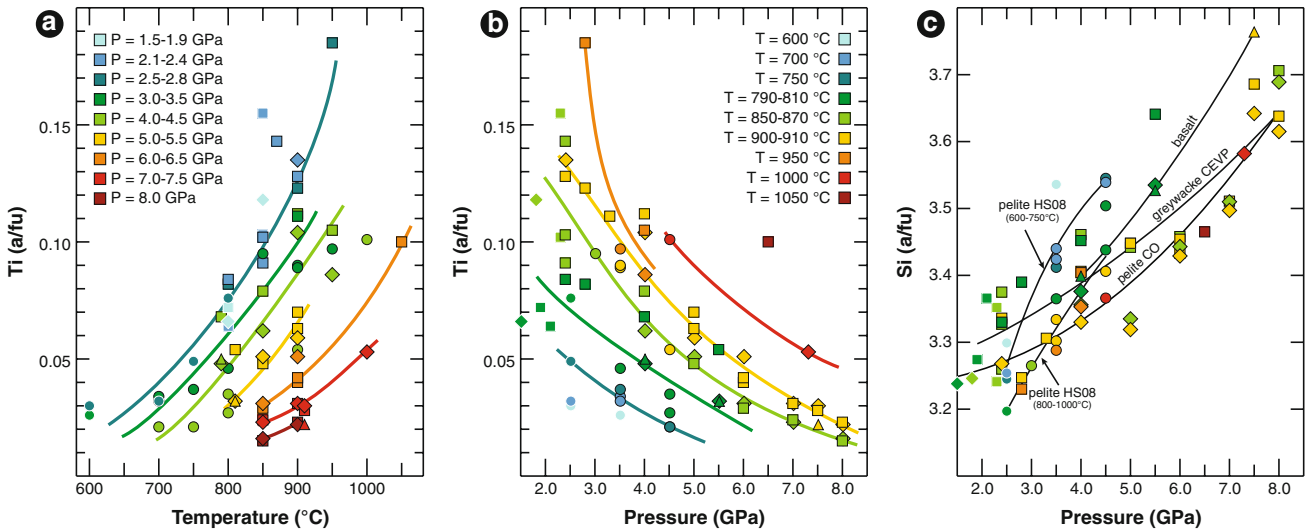

Fig. 6 Ti content in phengite as a function of temperature (**a**) and pressure (**b**) and Si content as a function of pressure (**c**). *Square* greywacke CEVP (this study), *diamond* pelite CO (this study), *triangle* K-rich MOR basalt (Schmidt et al. 2004), *circle* pelite (Hermann and Spandler 2008). Note the temperature effect and the drastic decrease of Ti between 1.9 and 8.0 GPa. The data from Hermann and Spandler (2008) and Schmidt et al. (2004) demonstrate that such evolutions apply for different rutile and quartz/coesite saturated rocks

with temperature except in the dataset of Hermann and Spandler (2008), which show an isobaric decrease in Si-content (see their Fig. 6a). These differences demonstrate that in the typical 4–6 phase assemblages of eclogites (phengite + garnet + cpx + quartz/coesite ± kyanite ± rutile), the bulk rock composition remains an important parameter controlling phengite composition and that the interpretation of Si content in natural phengites is more complicated than assumed in many previous geobarometers.

Thermodynamic modelling of the Ti-bearing phengite solid solution

Qualitatively, our results demonstrate that Ti-rich phengite in rutile- and quartz/coesite-saturated metamorphic rocks is a potential indicator of *P*–*T* conditions of equilibration in HP metamorphic rocks. The Ti-content of phengite is ideally suited as a geobarometric indicator because (i) many metamorphic rocks are TiO_2- and SiO_2-saturated, (ii) rutile and phengite have large overlapping stability fields, and (iii) the Ti-content of phengite is both temperature and pressure sensitive (Fig. 7). Coupled with an accurate thermometer such as the Ti content of zircon (Watson et al. 2006), Ti-rich phengite may represent a precise geobarometer (Fig. 7). This possibility motivates the quantitative treatment undertaken here. In our rutile and quartz/coesite saturated experiments, Ti content and celadonite component are inversely correlated and pressure sensitive. Thus, the knowledge of the MgCel + Rt = TiP + Cs/Qz equilibrium is essential to determine crystallization conditions of Ti-rich phengite-bearing metamorphic rocks saturated in rutile and quartz or coesite.

General approach

For a given pressure, temperature and phengite composition the following equations describe the aforementioned equilibrium:

$$G^{\mathrm{TiP}^\circ}_{T_1,P_1} + G^{\mathrm{Qz/Cs}^\circ}_{T_1,P_1} - G^{\mathrm{MgCel}^\circ}_{T_1,P_1} - G^{\mathrm{Rt}^\circ}_{T_1,P_1} + \mathrm{RT}_1 \ln K_{\mathrm{eq}} = 0$$

with

$$G^{\circ}_{T_1,P_1} = \Delta H_{T_{\mathrm{ref}},P_{\mathrm{ref}}} + \int_{T_{\mathrm{ref}}}^{T_1} Cp\mathrm{d}T - T_1\left(S_{T_{\mathrm{ref}},P_{\mathrm{ref}}} + \int_{T_{\mathrm{ref}}}^{T_1} \frac{Cp}{T}\mathrm{d}T\right) + \int_{P_{\mathrm{ref}}}^{P_1} V\mathrm{d}P$$

and

$$\mathrm{RT}_1 \ln K_{\mathrm{eq}} = \mathrm{RT}_1 \ln \frac{a^{id}_{\mathrm{TiP}}}{a^{id}_{\mathrm{MgCel}}} + \mathrm{RT}_1 \ln \frac{\gamma^{\mathrm{TiP}}}{\gamma^{\mathrm{MgCel}}}$$

The free energy of pure aluminoceladonite, rutile, coesite and quartz is calculated from the thermodynamic database of Holland and Powell (1998) updated by Coggon and Holland (2002). Thermodynamic properties of Ti-phengite are unknown and estimated from a linear combination of the Cp-functions of ferro-aluminoceladonite (FeCel), geikielite (Geik) and ferrosilite (Fs) using the relation

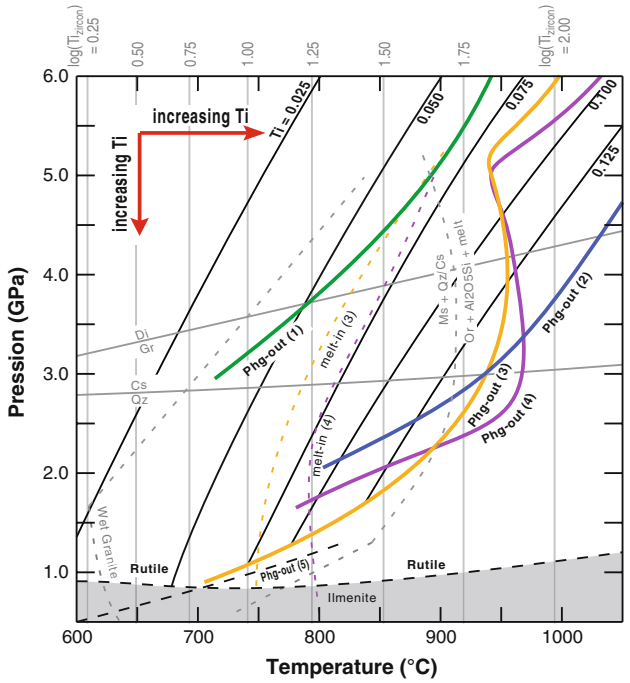

Fig. 7 The large overlapping stability fields of phengite and rutile (+qtz/coes) and the pressure sensitivity of Ti content, make Ti-rich phengite, a good candidate to determine the pressure of crystallisation of any rutile-coesite/quartz saturated metamorphic rock. *Black lines* iso-Ti-content in phengite (a/fu), *Green, blue, yellow* and *pink lines* high-temperature stability limits of phengite from different experimental studies; *yellow* and p*ink dashed lines* solidi. *(1)* Schmidt et al. (2004)—K-rich MORB, *(2)* Hermann and Spandler (2008)—pelite, *(3)* Vielzeuf and Holloway (1988) and Auzanneau (2005)—pelite CO, *(4)* Auzanneau et al. (2006)—greywacke CEVP. Iso-log(Ti_{zircon}) lines after Watson et al. (2006). Reaction Di = Gr after Liu (2002). *Black dashed lines* Calculated phengite stability limit *(5)* and stability fields of Ti-phases for the CEVP greywacke composition (calculated from Holland and Powell 1998). Reaction Ms + Qz/Cs = Or + Al_2SiO_5 + melt after Storre (1972), Huang and Wyllie (1974), Arnoult (1998) and Perier (1999). Wet granite solidus after Huang and Wyllie (1973)

TiP = 1FeCel + 1Geik − 0.5Fs. Holland and Powell (1998) assume that the thermal expansion parameter a° is the same for muscovite, aluminoceladonite and ferro-aluminoceladonite. Thus, the same value of a° is used for the Ti-phengite end-member. For dioctahedral micas, the incompressibility should increase with the Si content (Zanazzi and Pavese 2002). The muscovite and Ti-phengite end-members have both 3 Si per formula unit; thus we assume that the bulk modulus κ at 298 K of Ti-phengite is equal to that of muscovite. The reminder of the thermodynamic properties, i.e. molar enthalpy of formation, entropy and volume, are then calculated from least-squares regressions using experimental data.

For these calculations quartz and rutile are assumed to be pure and the mixing in phengite is modelled as non-ideal following the model of Coggon and Holland (2002). We

Table 4 Structural formula of phengite end-members and site partitioning scheme

	T1	T2	M1	M2A	M2B	A
Muscovite (Ms)	SiAl	SiSi	–	Al	Al	K
Paragonite (Pa)	SiAl	SiSi	–	Al	Al	Na
Ferri-muscovite (Fms)	SiAl	SiSi	–	Al	Fe^{3+}	K
Aluminoceladonite (MgCel)	SiSi	SiSi	–	Mg	Al	K
Ferro-aluminoceladonite (FeCel)	SiSi	SiSi	–	Fe^{2+}	Al	K
Ti-phengite (TiP)	SiAl	SiSi	–	Mg	Ti	K
Phlogopite (Phl)	SiAl	SiSi	Mg	Mg	Mg	K
Pyrophyllite (Prl)	SiSi	SiSi	–	Al	Al	–

also assume that (i) Mn and Ca are insignificant, (ii) the ionic ferric–ferrous ratio is unity, and (iii) the hydroxyl site contains only hydroxyl anions. With these assumptions eight end-members describe the composition of our experimental phengites: muscovite, paragonite, ferri-muscovite, pyrophyllite, ferro-aluminoceladonite, Mg-aluminoceladonite, Ti-phengite and phlogopite (Table 4). Coggon and Holland (2002) assume the ordering of Al onto the T1 tetrahedral sites to satisfy Al-avoidance (Holland and Powell 1990) and short range ordering onto M2A and M2B octahedral sites (Holland and Powell 1998). Here we assume that Ti occupies only the M2B site for the TiP endmember composition. The expression of the ideal activities and ideal activity ratio are then:

$$a^{id}_{\mathrm{MgCel}} = \left(X^{T1}_{\mathrm{Si}}\right)^2 \cdot \left(X^{T2}_{\mathrm{Si}}\right)^2 \cdot X^{M1}_{v} \cdot X^{M2A}_{\mathrm{Mg}} \cdot X^{M2B}_{\mathrm{Al}} \cdot X^{A}_{K}$$

$$a^{id}_{\mathrm{TiP}} = 4 \cdot X^{T1}_{\mathrm{Si}} \cdot X^{T1}_{\mathrm{Al}} \cdot \left(X^{T2}_{\mathrm{Si}}\right)^2 \cdot X^{M1}_{v} \cdot X^{M2A}_{\mathrm{Mg}} \cdot X^{M2B}_{\mathrm{Ti}} \cdot X^{A}_{\mathrm{K}}$$

$$\frac{a^{id}_{\mathrm{TiP}}}{a^{id}_{\mathrm{MgCel}}} = 4 \cdot \frac{X^{M2B}_{\mathrm{Ti}} \cdot X^{T1}_{\mathrm{Al}}}{X^{M2B}_{\mathrm{Al}} \cdot X^{T1}_{\mathrm{Si}}}$$

With

$X^{T1}_{\mathrm{Si}} = \frac{\mathrm{Si}-2}{2}$
$X^{T1}_{\mathrm{Al}} = \frac{4-\mathrm{Si}}{2}$
$X^{T2}_{\mathrm{Si}} = 1$
$S = \mathrm{Si} + \mathrm{Ti} + \mathrm{Al} + \mathrm{Fe}^{3+} + \mathrm{Fe}^{2+} + \mathrm{Mg}$
$X^{M1}_{\mathrm{Mg}} = S - 6$
$X^{M1}_{v} = 7 - S$
$X^{M2A}_{\mathrm{Al}} = 2\mathrm{S} - \mathrm{Fe}^{2+} - \mathrm{Mg} - 11$
$X^{M2A}_{\mathrm{Fe}^{2+}} = \mathrm{Fe}^{2+}$
$X^{M2A}_{\mathrm{Mg}} = \mathrm{Mg} + 12 - 2\mathrm{S}$
$X^{M2B}_{\mathrm{Ti}} = \mathrm{Ti}$
$X^{M2B}_{\mathrm{Al}} = 7 - (\mathrm{S} + \mathrm{Ti} + \mathrm{Fe}^{3+})$
$X^{M2B}_{\mathrm{Fe}^{3+}} = \mathrm{Fe}^{3+}$
$X^{M2B}_{\mathrm{Mg}} = \mathrm{S} - 6$
$X^{A}_{\mathrm{Na}} = \mathrm{Na}$
$X^{A}_{\mathrm{K}} = \mathrm{K}$
$X^{A}_{v} = 1 - (\mathrm{Na} + \mathrm{K})$

For the eight end-members, a symmetrical solution model based on Coggon and Holland (2002) is used. The regular solution is taken macroscopically and uses the molar fractions of the end-members for the calculation of activity coefficients (Holland and Powell 2003):

$$\mathrm{RT} \ln \gamma^{l} = -\sum_{i=1}^{n-1} \sum_{j>1}^{n} q_i \cdot q_j \cdot W^{*}_{ij}$$

with $q_i = 1 - \Phi_i$ when $i = l$ and $q_i = -\Phi_i$ when $i \neq l$

$$\Phi_i = \frac{x_i \cdot V_i}{\sum_i x_i \cdot V_i}$$

$$W^*_{ij} = W_{ij} \cdot 2 \cdot V_l \cdot \left(V_i + V_j\right)$$

$V_i = 0.63$ for all the potassic end-members (Ms, Fms, MgCel, FeCel, Phl, TiP); $V_{\mathrm{Pa}} = 0.37$ and $V_{\mathrm{Prl}} = 0.50$ (Coggon and Holland 2002) and

$$X_{\mathrm{Ms}} = 10 - \left(\mathrm{S} + \mathrm{Si} + \mathrm{Ti} + \mathrm{Fe}^{3+} + \mathrm{Na}\right)$$

$$X_{\mathrm{Pa}} = \mathrm{Na}$$

$$X_{\mathrm{Fms}} = \mathrm{Fe}^{3+}$$

$$X_{\mathrm{MgCel}} = \mathrm{Mg} + 18 - (3 \cdot \mathrm{S} + \mathrm{Ti})$$

$$X_{\mathrm{FeCel}} = \mathrm{Fe}$$

$$X_{\mathrm{TiP}} = \mathrm{Ti}$$

$$X_{\mathrm{Phl}} = \mathrm{S} - 6$$

$$X_{\mathrm{Prl}} = 1 - (\mathrm{Na} + \mathrm{K})$$

Coggon and Holland (2002) could not constrain the $W_{\mathrm{Phl–MgCel}}$ and $W_{\mathrm{Fms–MgCel}}$ binary interaction coefficients and arbitrary set them to zero. For the same reason, the $W_{\mathrm{Fms–TiP}}$ binary coefficient is also set to zero. The solid solution FeCel–MgCel is ideal ($W_{\mathrm{FeCel–MgCel}} = 0$; Coggon and Holland 2002) thus $W_{\mathrm{MgCel–TiP}}$ and $W_{\mathrm{FeCel–TiP}}$ are supposed to be equal. The activity coefficient ratio is then:

$$\begin{aligned} \mathrm{RT} \ln \frac{\gamma^{\mathrm{TiP}}}{\gamma^{\mathrm{MgCel}}} = {} & \Phi_{\mathrm{Ms}} \left(W^*_{\mathrm{Ms–TiP}} - W^*_{\mathrm{Ms–MgCel}}\right) \\ & + \Phi_{\mathrm{Pa}} \left(W^*_{\mathrm{Pa–TiP}} - W^*_{\mathrm{Pa–MgCel}}\right) \\ & + \Phi_{\mathrm{Prl}} \left(W^*_{\mathrm{Prl–TiP}} - W^*_{\mathrm{Prl–MgCel}}\right) \\ & + \left(\Phi_{\mathrm{MgCel}} + \Phi_{\mathrm{FeCel}} - \Phi_{\mathrm{TiP}}\right) \cdot W^*_{\mathrm{MgCel–TiP}} \end{aligned}$$

The V_i, $W_{\mathrm{Ms–MgCel}}$, $W_{\mathrm{Pa–MgCel}}$ and $W_{\mathrm{Prl–MgCel}}$ values are from Coggon and Holland (2002) while the $W_{\mathrm{Ms–TiP}}$; $W_{\mathrm{Pa–TiP}}$; $W_{\mathrm{Prl–TiP}}$ and $W_{\mathrm{MgCel–TiP}}$ are determined along with the thermodynamic parameters of Ti-phengite by multiple linear regression of the experimental data. $W_{\mathrm{Ms–TiP}}$, $W_{\mathrm{Pa–TiP}}$, $W_{\mathrm{Prl–TiP}}$ and $W_{\mathrm{MgCel–TiP}}$ are assumed to be independent of P and T. The expression of the minimized function is given in Appendix 1.

Experimental data set and regression procedure

Thirty experiments from the metagreywacke CEVP and 18 from the metapelite CO are used for the modelling. Furthermore, the data include the 19 experimental results of Hermann and Spandler (2008; HS) for pelitic bulk compositions and the 3 experimental results of Schmidt et al. (2004) for basaltic compositions. To correct some irregularities related to small stoichiometric defects in some phengites, minor adjustments have been necessary. In some cases, $\sum \mathrm{cat.}^{\mathrm{XII}} > 1$ or $\sum \mathrm{cat.}^{\mathrm{VI}} < 2$ and thus it was not possible to describe properly the phengite composition by the 8 selected end-members. Thus, the Fe^{3+} proportion was adjusted in the limited range 25–75% of Fe_{total} in order to get $\sum \mathrm{cat.}^{\mathrm{XII}} \leq 1$, $\sum \mathrm{cat.}^{\mathrm{VI}} \geq 2$, and thus X_{Prl} and $X_{\mathrm{Phl}} \geq 0$. When proper values could such not be obtained, the slightly negative end-member molar fraction was set to zero and the molar fractions were normalised. After correction of the end-member molar fractions, the structural formulae and the site distribution of the elements were recalculated. A comparison between initial and corrected analyses demonstrates that such corrections are minimal and remain smaller than analytical errors.

To identify and exclude the effect of outlier observations, we employed an iterative regression scheme in which any observation with residuals outside of the 95% confidence interval for the residual based on the regression model was rejected. The regression and outlier tests were repeated until no new outliers were identified. Likewise, if the 95% confidence interval on a model parameter was found to include zero, the parameter was set to zero and not further used in the model. Regression models were only considered to be acceptable if the Fischer F-statistic showed the overall model to be significant at 95% confidence level.

Results

The iterative regression process eliminates 10 of the 70 sets in our dataset. Four sets, come from experiments carried out between 1.5 and 2.1 GPa, i.e. the lowest experimental pressures (PC3-2001-13$_{\mathrm{CEVP}}$; PC3-2001-12$_{\mathrm{CEVP}}$; PC2-2002-26$_{\mathrm{CO}}$ and PC3-2002-1$_{\mathrm{CO}}$). Six other sets were rejected because of analytical problems: the high CaO concentration (0.31 wt%) present in the phengite from the experiment C-2082D$_{\mathrm{HS}}$, performed at 3.5 GPa and 600°C, reveals a probable contamination by the surrounding phases during the analysis. Compared to the general compositional trends observed in Fig. 4, the very low Al and high Si contents in ME107$_{\mathrm{CEVP}}$ (5.5 GPa–810°C), the extremely high FeO concentration in ME95$_{\mathrm{CO}}$ (7.3 GPa—1,000°C) and the very high TiO_2 content in ME96$_{\mathrm{CEVP}}$ (6.5 GPa—1,050°C) reveal a possible incomplete equilibration during the experiment or contamination during the analysis. In addition, the significant differences in composition between the C-2596$_{\mathrm{HS}}$ (eliminated experiment) and the C-1872a$_{\mathrm{HS}}$ performed from the same starting material and at the same P–T conditions (4.5 GPa—800°C) demonstrate an incomplete equilibration in the C-2596$_{\mathrm{HS}}$ experiment or an analytical contamination. There is no obvious explanation for the outlier behaviour of the C-2590D$_{\mathrm{HS}}$ (4.5 GPa-750°C). During the regression, the $W_{\mathrm{Ms–TiP}}$ parameter did

not pass the t test. Thus, this mixing parameter is not significant for the model and is set to zero. There is no significant correlation between the model residuals and phengite composition, molar fractions of end members, or experimental conditions.

The molar thermodynamic parameters obtained from our modelling are:

$$\Delta H_{\underset{T_{ref},P_{ref}}{TiP}} = -5869180 \pm 4000 \text{ (J)}$$

$$S_{\underset{T_{ref},P_{ref}}{TiP}} = 318.9 \pm 3.4 \text{ (J/K)}$$

$$V_{\underset{T_{ref},P_{ref}}{TiP}} = 14.740 \pm 0.035 \text{ (J/bar)}$$

$$W_{MgCel-TiP} = W_{FeCel-TiP} = 10,000 \pm 2,000 \text{ (J/mol)}$$

$$W_{Ms-TiP} = 0 \text{ (J/mol)}$$

$$W_{Pa-TiP} = 80{,}000 \pm 8{,}000 \text{ (J/mol)}$$

$$W_{Prl-TiP} = 40{,}000 \pm 5{,}000 \text{ (J/mol)}.$$

An inverse test in which the experimental conditions are back-calculated from the regression model shows good agreement. The concordance between the experimental temperatures and the temperatures calculated at experimental pressure is satisfactory ($R^2 = 0.85$ and $\overline{\left\|\frac{100\times\Delta T}{T_{exp}}\right\|} = 3.3\%$, Fig. 8a) and the pressures calculated at experimental temperatures are also in good agreement with experimental pressures ($R^2 = 0.97$ and $\overline{\left\|\frac{100\times\Delta P}{P_{exp}}\right\|} = 6.2\%$, Fig. 8b). As with the Gibbs free energy, no correlation between the calculated deviations ΔT or ΔP and phengite compositions, end-member molar fractions or experimental conditions has been observed. The absence of significant correlations indicates that no additional P-, T- or X-dependent terms are justified.

Effect of Fe^{3+}

Following an identical procedure, regressions have been undertaken assuming $Fe^{3+} = 0\%$ and $Fe^{3+} = 20\%$ of the total Fe. The thermodynamic parameters obtained from these fits are not drastically different than for the fit assuming $Fe^{3+} = 50\%$ (Appendix 2). The concordance between the experimental temperatures and the calculated ones are similar to those derived with $Fe^{3+} = 50\%$ ($Fe^{3+} = 0\%$: $R^2 = 0.86$ and $\overline{\left\|\frac{100\times\Delta T}{T_{exp}}\right\|} = 3.3\%$; $Fe^{3+} = 20\%$: $R^2 = 0.86$ and $\overline{\left\|\frac{100\times\Delta T}{T_{exp}}\right\|} = 3.4\%$), while the concordance between the experimental pressures and the calculated ones are slightly less good than previously ($Fe^{3+} = 0\%$: $R^2 = 0.95$ and $\overline{\left\|\frac{100\times\Delta P}{P_{exp}}\right\|} = 8.0\%$; $Fe^{3+} = 20\%$: $R^2 = 0.95$ and $\overline{\left\|\frac{100\times\Delta P}{P_{exp}}\right\|} = 8.3\%$). From this, we conclude, that, within the bounds of 0–50% Fe^{3+}, the thermodynamic fit and the subsequent geobarometric calculations are little affected by the choice of Fe-oxidation state, as long as a coherent normalization scheme is applied to the experiments and the natural samples. We thus suggest to employ a value of 50% Fe^{3+} in accordance with the

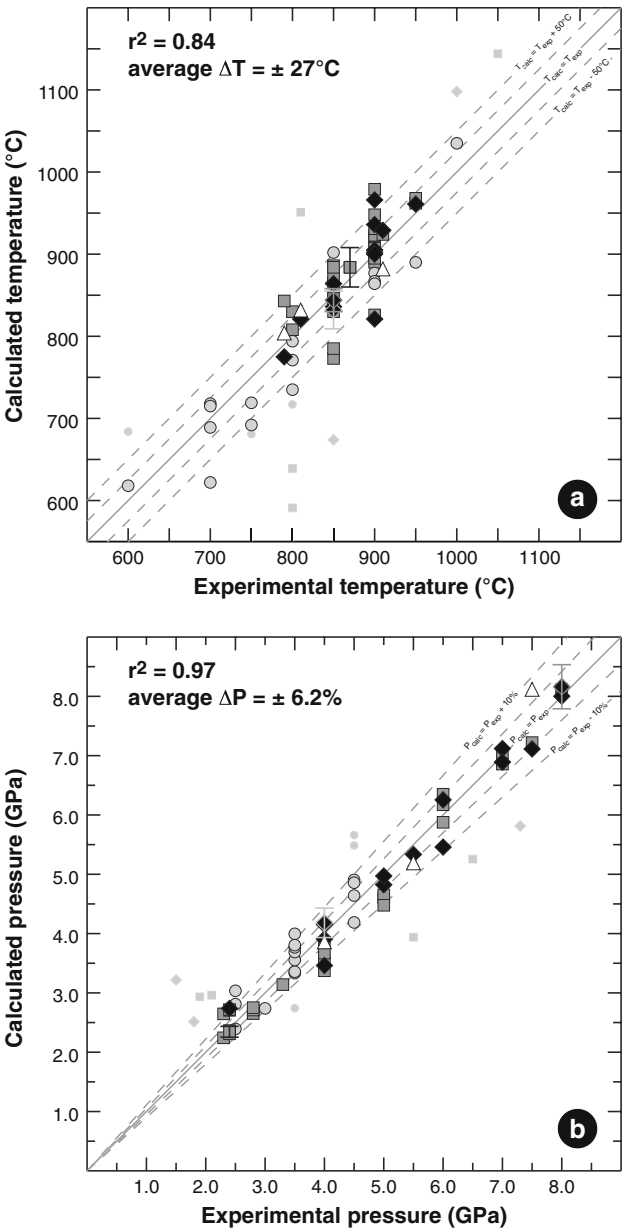

Fig. 8 **a** Calculated temperatures at experimental pressure versus experimental temperatures. **b** Calculated pressures at experimental temperatures versus experimental pressures. *Square* greywacke CEVP (this study), *diamond* pelite CO (this study), *triangle* K-rich MOR basalt (Schmidt 2004), *circle* pelite (Hermann and Spandler 2008), *small symbol* discarded experiment. *Error bars* calculated by a Monte Carlo method are reported for three experiments. Because the reaction slope increases with P and T, the absolute error on the calculated pressure increases with the experimental pressure, while errors on temperature decrease

few existing direct measurements (Guidotti and Sassi 1998a; Schmid et al. 2003).

Application to natural samples—discussion

Phengite, rutile and coesite or quartz are common minerals in HT-(U)HP felsic and basic metamorphic rocks. For such samples, the MgCel-Rt-TiP-Cs/Qz equilibrium calibrated at high temperature over a wide range of pressure can be used to determine crystallization conditions. Here, we present examples from two UHP metamorphic massifs (Sulu Terrain, China and Kokchetav Massif, Kazakhstan). The Sulu metamorphic area is the largest exposed UHP unit and numerous analyses from gneissic and eclogitic rocks are available from previous work. The Kokchetav is the area where the most extreme *P–T* conditions for continental crustal rocks known to date have been reported.

The supracrustal rock unit of the southern Sulu belt (China) is interpreted as a huge volume of continental material subducted to depths > 100 km, and then exhumed to the surface (Liu et al. 2004). The Sulu belt is mainly composed of gneiss containing thin layers of quartzites, schists, eclogites, and ultramafic rocks. In the Donghai area, south-western Sulu terrane, the maximum pressure estimates range from 3.0 to 4.4 GPa (Zhang et al. 2000, Zhang et al. 2005a, b, 2006a, b) and calculated temperatures are comprised between 630 (Zhang et al. 2002a, b) and 890°C (Liu et al. 2004). The retrograde *P–T* path is characterised by a slight temperature decrease (Zhang et al. 2005a, b). This area has been extensively studied during the last 20 years and many studies provide phengite analyses from gneisses and eclogites (Zhang et al. 2000, 2005a, b, 2006a, b; Liu et al. 2001, 2002, 2003; Cosca et al. 2005).

Micas from the felsic samples (gneisses and few schists and quartzites) cover a very wide range of compositions and no distinction can be made between rutile-bearing samples and samples where no rutile has been reported. The SiO_2 concentrations vary over a large interval (44–54 wt%) while TiO_2 is low and does not change drastically (Fig. 9a). The phengites trapped in zircon with coesite (red dots) are the richest in Si as they were protected from reequilibration during regression and thus are particularly interesting for this study. The average pressure calculated at 750°C from three phengites trapped in zircon with coesite and rutile (Liu et al. 2001, 2002) is 6.0 ± 0.4 GPa (Fig. 10a).

Micas from mafic rocks (eclogites and amphibolites) also show a wide and continuous range of compositions and are characterised by uniformly low Ti-contents and by the lack of correlation between Si and Ti (Fig. 9b). The calculated pressure at 750°C from the two phengites trapped with coesite (Liu et al. 2003) at UHP is 5.3 ± 0.4 GPa.

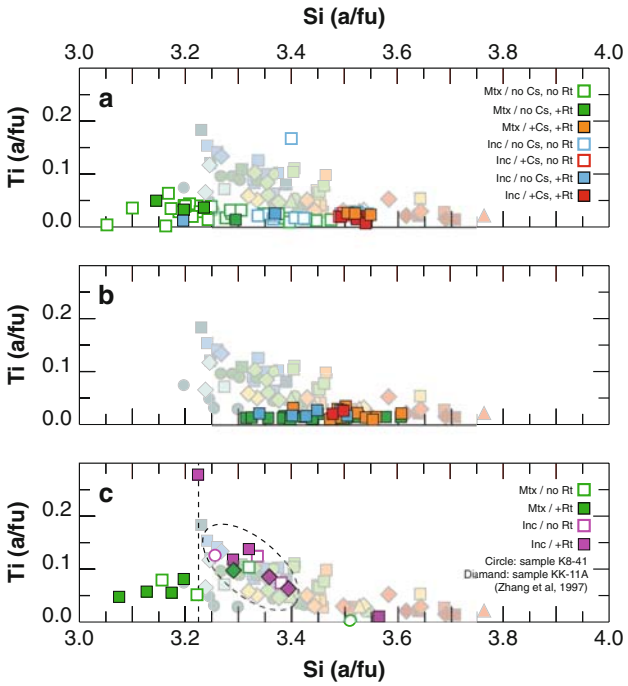

Fig. 9 Ti versus Si. **a** Felsic samples from the Sulu belt, **b** basic metamorphic rocks from the Sulu belt, **c** Gneisses from the Kokchetav Massif. *Light dots* experimental data

Some phengites from the matrix of other samples are richer in Si (up to 3.6 Si/fu—Zhang et al. 2000; Cosca et al. 2005) and lead to slightly higher pressure estimation (5.7 ± 0.5 GPa).

These estimates are significantly higher than those available in the literature. There are five possible explanations. (1) The choice of 750°C as average temperature is good, and pressures are that high. This would imply a thermal gradient (125–140°C/GPa ≈ 3.3–3.7°C/km) less than the lower limit for UHP metamorphism observed in nature (150°C/GPa; Brown 2007), which is unrealistic. (2) The assumed Fe^{3+}/Fe^{2+} ratio is too high and leads to erroneous calculated pressure. Complementary calculation was performed considering $Fe^{3+} = 0$ and 20% of the total Fe. Calculated pressures are slightly shifted towards lower values (by about −0.2 GPa) and thus remain essentially unchanged. The Fe^{3+}/Fe^{2+} ratio does not seem to be a crucial parameter. (3) The temperatures assumed from thermobarometry are very high resulting in a calculated peak pressure shifted towards high values. Considering the lowest estimated temperatures (≈680°C—Zhang et al. 2002a, b; Liu et al. 2003; Zhang et al. 2006a, b), the calculated pressures become 4.4 ± 0.3 and 3.9 ± 0.3 GPa (Fig. 10a), respectively with felsic and basic samples. This corresponds to a thermal gradient of 140–160°C/GPa (≈3.7–4.3°C/km). These gradients are more realistic but such *P–T* conditions do not fit on typical *P–T* paths such

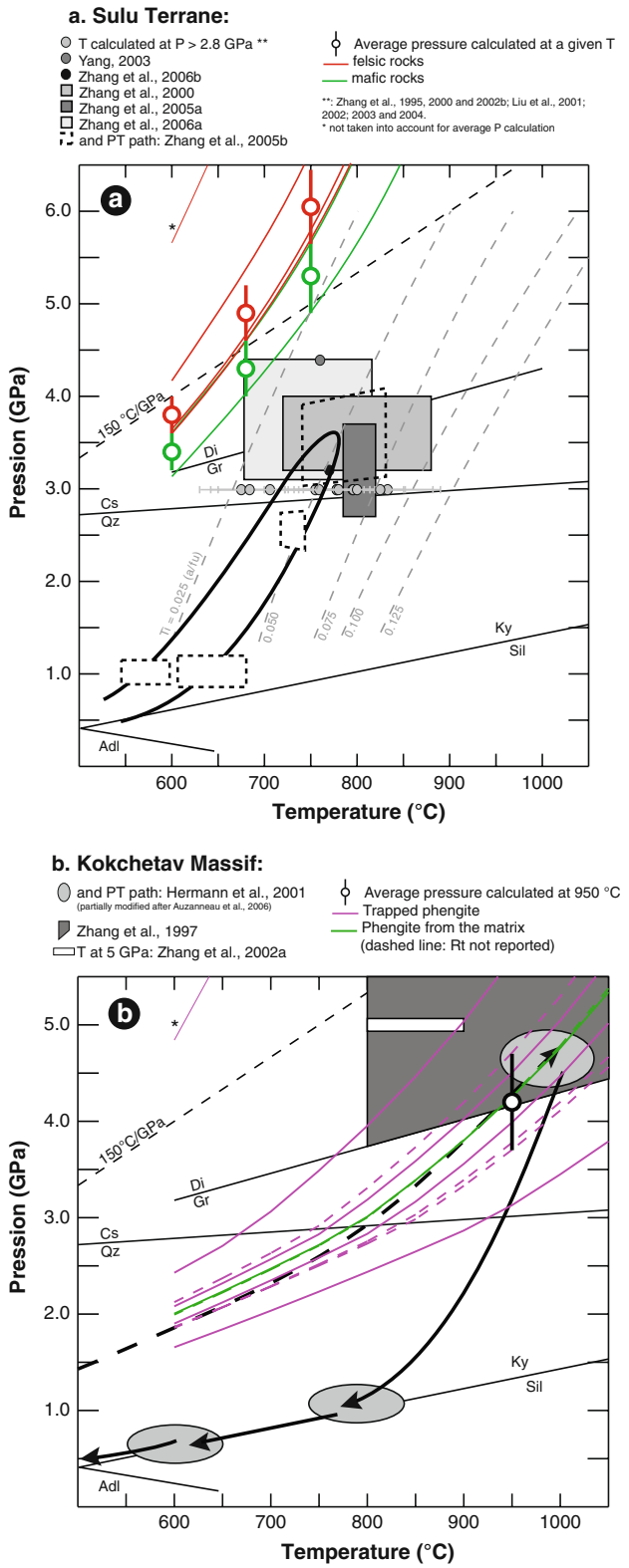

Fig. 10 Location in the *P–T* space of the MgCel–Rt–TiP–Cs/Qz equilibriums calculated from the composition of natural phengite from the Sulu belt (**a**) and the Kokchetav Massif (**b**). For discussion see text

as the one proposed by Zhang et al. (2005a, b). Our pressure calculations would then imply a temperature increase during exhumation and corroborate the proposal of Liu et al. (2006) that UHP-terrains do not simultaneously arrive at maximum pressure and temperature, but that peak pressure significantly predates peak temperature. (4) The phengites were trapped before the peak pressure, in the coesite stability field, at even lower temperatures. The experimental data indicate that the low Ti content (<0.03 a/fu) in these phengites trapped with coesite and rutile in the zircon grains are compatible with relatively HP and LT conditions. Considering a hypothetical trapping temperature of 600°C, the calculated pressure is about 3.6 GPa. This result leads to a subduction *P–T* path divided into two stages: a cold subduction followed by important heating at UHP. (5) The composition of the phengites are not representative of the conditions of entrapment in the zircon. The generally low Ti contents in the phengite, the existence of zoned grains in the matrix (Giorgis et al. 2000; Cosca et al. 2005; Zhang et al. 2006a, b) and the heterogeneous composition of phengite inclusions trapped with coesite in the same growth zone of a zircon grain (Liu et al. 2001; their sample C121) point out an incomplete equilibration of the phases at the moment of the entrapment. In this scenario, trapped phengites could have crystallised during an early stage of metamorphism, they may have preserved a metastable composition until entrapment at different *P–T* conditions. This hypothesis, consistent with independent petrological observations may lead to reconsider the significance of inclusions trapped in zircons as proxies of peak *P* and *T* conditions of metamorphism.

Diamondiferous gneisses and schists from the Kokchetav Massif (Kazakhstan) represent another example of continental rocks deeply subducted and rapidly exhumed to shallow depth. In these rocks, K-white mica was an ubiquitous mineral during a large part of the metamorphic history, which included three main crystallisation stages: $P > 4.3$ GPa, $T \approx 950$°C; $P \approx 1.0$ GPa, $T \approx 800$°C and $P \approx 0.5$ GPa, $T \approx 600$°C (Fig. 10b, Hermann et al. 2001, partially modified after Auzanneau et al. 2006). Phengite grains are commonly observed as inclusions in both garnet and zircon or as a matrix phase. Published analyses (Vavilov et al. 1991; Shatsky et al.. 1995; Zhang et al. 1997; Hermann et al. 2001; Zhang et al. 2002a, b; Massonne 2003) show a large range of composition which arises from the changes of *P–T* conditions and the variability in protolith compositions. In a Ti versus Si diagram (Fig. 9c), two groups of K-white micas are identified. The first one is composed of Si-rich phengites (Si > 3.25 a/fu) showing an inverse correlation between

Ti and Si, as in our experiments. No distinction can be made between samples in which rutile has or has not been reported. This lack of difference suggests that rutile may have been present (but not noted) with the Si-rich phengites in all samples and buffered Ti contents in the phengitic micas. Compared to our experimental data, these natural Si-rich phengites are in the same range of composition (except that they are poorer in Na) and they are good candidates for determining pressures of crystallisation. Among the 12 analyses, three are significantly different from the others by their either low or high Ti content. The two Ti-poorest ones (Ti = 0.001 and 0.012 a/fu) are Si-rich (>3.5 a/fu) and are respectively characterised by high $\sum$cat.^{IV} (2.20 a/fu) and low $\sum$cat.^{XII} (0.75 a/fu). The Ti-richest phengite (TiO_2 = 5.62 wt%) is characterised by Mg + Fe < Ti, a low K content and $\sum$cat.^{XII} = 0.75 a/fu, which is significantly lower than the ideal value. The fact that Mg + Fe is lower than Ti means that the Ti content cannot be balanced solely by the substitution we propose here. Thus, these phengites were discarded from the first group. In the other group of micas, phengites are poorer in Si (Si < 3.25 a/fu), Ti contents are low and the previous negative correlation with Si does not apply (Fig. 9c). These grains can be related to late metamorphic stages and are not taken into account to calculate peak metamorphic conditions.

The results of calculations performed with the nine remaining Si-rich analyses are shown in Fig. 10b. The location of the calculated equilibria in *P–T* space is homogenous and the average pressure calculated at 950°C is 4.2 ± 0.5 GPa. This quantitative estimate of crystallisation pressure is consistent with the presence of diamonds reported by Sobolev and Shatsky (1990).

Conclusion

Our results show that in felsic (and basic) rocks with rutile and quartz/coesite, Ti can be a significant constituent of phengites equilibrated at HT-(U)HP. As Ti influences the Si-content of micas via charge coupled substitutions, Si by itself is not as reliable as a pressure indicator in phengitic micas as has been commonly assumed.

The present experimental study and thermodynamic modelling demonstrate that Ti-rich phengite coexisting with rutile and quartz/coesite is a valuable tool to determine the pressure of crystallisation of HT-(U)HP metamorphic rocks. These rocks are generally affected by recrystallisation processes during exhumation, which renders the determination of peak metamorphic conditions difficult. On the other hand, mineral inclusions (including phengites) in zircon or garnet may witness peak metamorphism or earlier stages of metamorphism (Chopin 2003). Combining the zircon Ti thermometer (Watson et al. 2006; Ferry and Watson 2007) and the MgCel–Rt–TiP–Qz/Cs barometer, on phengite inclusions in zircon is a way to determine the *T–P* conditions prior to retrogression. However, the example of Sulu shows that even in that case the interpretation of the results remains difficult. This could be due to kinetic effects and the inability of a solid-solutions such as phengite to maintain permanent chemical equilibrium as pressure and temperature change through time. Alternatively, peak temperatures could generally be achieved after peak pressures, which due to prograde equilibration remains difficult to demonstrate.

Experimental studies have highlighted the key role of phengite for the formation of melt (or supercritical liquid) during subduction related high *P–T* metamorphism (Domanik and Holloway 1996; Schmidt 1996; Schmidt et al. 2004) and during the exhumation of UHP metamorphic rocks (Hermann 2002; Auzanneau et al. 2006). By analogy with Ti in biotite, Ti in phengite could have significant effects on the solidus temperature, stability limit of phengite, and the melting rate with decreasing *P* or increasing *T*. Thus, differences in melting behaviour can be expected for Ti-poor and Ti-saturated rocks, with effects on the density and the rheology of the partially molten rocks and subsequently their exhumation.

Appendix 1

Expression of the minimized function

$$\begin{aligned}
&\left(\int_{T_{\mathrm{ref}}}^{T_2} Cp_{\mathrm{TiP}}\mathrm{d}T - T_2\left(\int_{T_{\mathrm{ref}}}^{T_2}\frac{Cp_{\mathrm{TiP}}}{T}\mathrm{d}T\right)\right)\\
&+ G^{\mathrm{Qz/Cs}^\circ}_{T_2,P_2} - G^{\mathrm{MgCel}^\circ}_{T_2,P_2} - G^{\mathrm{Rt}^\circ}_{T_2,P_2} + \mathrm{R}T_2\ln\frac{a^{id}_{\mathrm{TiP}}}{a^{id}_{\mathrm{MgCel}}}\\
&-\left[\Phi_{\mathrm{Ms}}\cdot W^*_{\mathrm{Ms-MgCel}} + \Phi_{\mathrm{Pa}}\cdot W^*_{\mathrm{Pa-MgCel}} + \Phi_{\mathrm{Prl}}\cdot W^*_{\mathrm{Prl-MgCel}}\right]\\
&= -\left[\Delta H^{\mathrm{TiP}}_{T_{\mathrm{ref}},P_{\mathrm{ref}}} - T_2\cdot \mathrm{S}^{\mathrm{TiP}}_{T_{\mathrm{ref}},P_{\mathrm{ref}}} + V^{\mathrm{TiP}}_{T_{\mathrm{ref}},P_{\mathrm{ref}}}\cdot F^{\mathrm{TiP}}_{T_2,P_2}\right]\\
&-\left[\Phi_{\mathrm{Ms}}\cdot W^*_{\mathrm{Ms-TiP}} + \Phi_{\mathrm{Pa}}\cdot W^*_{\mathrm{Pa-TiP}} + \Phi_{\mathrm{Prl}}\cdot W^*_{\mathrm{Prl-TiP}}\right.\\
&\left.+\left(\Phi_{\mathrm{MgCel}} + \Phi_{\mathrm{FeCel}} - \Phi_{\mathrm{TiP}}\right)\cdot W^*_{\mathrm{MgCel-TiP}}\right]
\end{aligned}$$

with

$$V^{\mathrm{TiP}}_{T_{\mathrm{ref}},P_{\mathrm{ref}}}\cdot F^{\mathrm{TiP}}_{T_2,P_2} = \int_{P_{\mathrm{ref}}}^{P_2} V_{\mathrm{TiP}}\mathrm{d}P$$

and

$$F_{\underset{T_2,P_2}{\mathrm{TiP}}} = \frac{\left(1 + a^0_{\mathrm{TiP}}(T_2 - T_{\mathrm{ref}}) - 20a^0_{\mathrm{TiP}}\left(\sqrt{T_2} - \sqrt{T_{\mathrm{ref}}}\right)\right)\kappa_{\mathrm{TiP}}(1 - 1.5 \times 10^{-4}(T_2 - T_{\mathrm{ref}}))}{3} \times \left[\left(1 + \frac{4P_2}{\kappa_{\mathrm{TiP}}(1 - 1.5 \times 10^{-4}(T_2 - T_{\mathrm{ref}}))}\right)^{3/4} - 1\right]$$

Right-hand side of the function: known values and left-hand side: unknown parameters $\Delta H_{\underset{T_{\mathrm{ref}},P_{\mathrm{ref}}}{\mathrm{TiP}}}$; $S_{\underset{T_{\mathrm{ref}},P_{\mathrm{ref}}}{\mathrm{TiP}}}$; $V_{\underset{T_{\mathrm{ref}},P_{\mathrm{ref}}}{\mathrm{TiP}}}$; $W_{\mathrm{Ms-TiP}}$; $W_{\mathrm{Pa-TiP}}$; $W_{\mathrm{Prl-TiP}}$; $W_{\mathrm{MgCel-TiP}}$ and input data (constraints)

T_2; P_2; $F_{\underset{T_2,P_2}{\mathrm{TiP}}}$; $\left(X_{\mathrm{MgCel}} + X_{\mathrm{FeCel}} - X_{\mathrm{TiP}}\right)$; X_{Ms}; X_{Pa}

Appendix 2

Molar thermodynamic parameters obtained at $Fe^{3+} = 0\%$:

$\Delta H_{\underset{T_{\mathrm{ref}},P_{\mathrm{ref}}}{\mathrm{TiP}}} = -5{,}863{,}800 \pm 4{,}000$ (J)

$S_{\underset{T_{\mathrm{ref}},P_{\mathrm{ref}}}{\mathrm{TiP}}} = 322.3 \pm 3.7$ (J/K)

$V_{\underset{T_{\mathrm{ref}},P_{\mathrm{ref}}}{\mathrm{TiP}}} = 14.700 \pm 0.037$ (J/bar)

$W_{\mathrm{MgCel-TiP}} = W_{\mathrm{FeCel-TiP}} = 12{,}500 \pm 2{,}000$

$W_{\mathrm{Ms-TiP}} = 0$ (J/mol)

$W_{\mathrm{Pa-TiP}} = 80{,}000 \pm 9{,}000$ (J/mol)

$W_{\mathrm{Prl-TiP}} = 40{,}000 \pm 6{,}000$ (J/mol).

Molar thermodynamic parameters obtained at $Fe^{3+} = 20\%$:

$\Delta H_{\underset{T_{\mathrm{ref}},P_{\mathrm{ref}}}{\mathrm{TiP}}} = -5{,}862{,}950 \pm 4{,}000$ (J)

$S_{\underset{T_{\mathrm{ref}},P_{\mathrm{ref}}}{\mathrm{TiP}}} = 323.0 \pm 3.7$ (J/K)

$V_{\underset{T_{\mathrm{ref}},P_{\mathrm{ref}}}{\mathrm{TiP}}} = 14.696 \pm 0.037$ (J/bar)

$W_{\mathrm{MgCel-TiP}} = W_{\mathrm{FeCel-TiP}} = 12{,}000 \pm 2{,}000$ (J/mol)

$W_{\mathrm{Ms-TiP}} = 0$ (J/mol)

$W_{\mathrm{Pa-TiP}} = 80{,}000 \pm 9{,}000$ (J/mol)

$W_{\mathrm{Prl-TiP}} = 40{,}000 \pm 6{,}000$ (J/mol).

References

Agard P, Vidal O, Goffe B (2001) Interlayer and Si content of phengite in HP-LT carpholite-bearing metapelites. J Metamorph Geol 19(5):477–493

Arnoult L (1998) Experimental melting of muscovite between 50 and 850 Kbar. Master thesis, Blaise Pascal, Clermont-Ferrand, France, p 28

Auzanneau E (2005) Experimental study of phase relations in metasedimentary rocks at high pressure and temperature; application to subducted continental crust. Doctor thesis. Université Blaise Pascal, Clermont-Ferrand, France, p 279

Auzanneau E, Vielzeuf D, Schmidt MW (2006) Experimental evidence of decompression melting during exhumation of subducted continental crust. Contrib Mineral Petrol 152(2):125–148

Biino GG, Compagnoni R (1992) Very-high pressure metamorphism of the Brossasco coronite metagranite, southern Dora Maira Massif, Western Alps. Schweiz Mineral Petrogr Mitt 72:347–363

Bishop FC, Smith JV, Dawson JB (1976) Na, P, Ti and coordination of Si in garnet from peridotite and eclogite xenoliths. Nature 260:696–697

Bishop FC, Smith JV, Dawson JB (1978) Na, K, P and Ti in garnet, pyroxene and olivine from perodotite and eclogite xenoliths from African kimberlites. Lithos 11:155–173

Brown M (2007) Metamorphic conditions in orogenic belts: a record of secular change. Int Geol Rev 49:193–234

Cawthorn RG, Collerson KD (1974) The recalculation of pyroxene end-member parameters and the estimation of ferrous and ferric iron content from electron microprobe analyses. Am Mineral 59(11–12):1203–1208

Cesare B, Cruciani G, Russo U (2003) Hydrogen deficiency in Ti-rich biotite from anatectic metapelites (El Joyazo, SE Spain); crystal-chemical aspects and implications for high-temperature petrogenesis. Am Mineral 88(4):583–595

Chopin C (2003) Ultrahigh-pressure metamorphism: tracing continental crust into the mantle. Earth Planet Sci Lett 212:1–14

Coggon R, Holland TJB (2002) Mixing properties of phengitic micas and revised garnet-phengite thermobarometers. J Metamorph Geology 20(7):683–696

Cosca MA, Giorgis D, Rumble D, Liou JG (2005) Limiting effects of UHP metamorphism on length scales of oxygen, hydrogen, and argon isotope exchange: an example from the qinglongshan UHP eclogites, Sulu Terrain, China. Int Geol Rev 47(7):716–749

Domanik KJ, Holloway JR (1996) The stability and composition of phengitic muscovite and associated phases from 5.5 to 11 GPa: Implications for deeply subducted sediments. Geochim Cosmochim Acta 60(21):4133–4150

Dyar MD, Guidotti CV, Holdaway MJ, Colucci M (1993) Nonstoichiometric hydrogen contents in common rock-forming hydroxyl silicates. Geochim Cosmochim Acta 57(12):2913–2918

Dyar MD, Lowe EW, Guidotti CV, Delaney JS (2002) Fe^{3+} and Fe^{2+} partitioning among silicates in metapelites; a synchrotron micro-XANES study. Am Mineral 87(4):514–522

Dymek RF (1983) Titanium, aluminum and interlayer cation substitutions in biotite from high-grade gneisses, West Greenland. Am Mineral 68(9–10):880–899

Ernst WG (1963) Significance of phengitic micas from low-grade schists. Am Mineral 48(11-2):1357

Ferraris G, Ivaldi G (2002) Structural features of micas. In: Mottana A, Sassi FP, Thompson JBJ, Guggenheim S (eds) Micas: crystal chemistry and metamorphic petrology, vol 46. Mineralogical Society of America and Geochemical Society, Washington, DC, pp 117–153

Ferry JM, Watson EB (2007) New thermodynamic models and revised calibrations for the Ti-in-zircon and Zr-in-rutile thermometers. Contrib Mineral Petrol 154:429–437

Giorgis D, Cosca M, Li SG (2000) Distribution and significance of extraneous argon in UHP eclogite (Sulu terrain, China): insight from in situ Ar-40/Ar-39 UV-laser ablation analysis. Earth Planet Sci Lett 181(4):605–615

Gouzu C, Itaya T, Takeshita H (2005) Interlayer cation vacancies of phengites in calcschists from the Piemonte zone, western Alps, Italy. J Mineral Petrol Sci 100(4):143–149

Guidotti CV (1978) Compositional variation of muscovite in medium- to high-grade metapelites of northwestern Maine. Am Mineral 63(9–10):878–884

Guidotti CV (1984) Micas in metamorphic rocks. In: Bailey SW (ed) Micas, vol 13. Mineralogical society of America, pp 357–467

Guidotti CV, Sassi FP (1998a) Miscellaneous isomorphous substitutions in Na-K white micas: a review, with special emphasis to metamorphisc micas. Rend Fis Acc Lincei 9(9):57–78

Guidotti CV, Sassi FP (1998b) Petrogenetic significance of Na–K white mica mineralogy; recent advances for metamorphic rocks. Eur J Mineral 10(5):815–854

Guidotti CV, Sassi FP (2002) Constraints on studies of metamorphic K–Na white micas. In: Mottana A, Sassi FP, Thompson JB, Guggenheim S (eds) Micas: crystal chemistry and metamorhpic petrology, vol 46. Mineralogical society of America, pp 413–448

Guidotti CV, Cheney JT, Guggenheim S (1977) Distribution of titanium between coexisting muscovite and biotite in pelitic schists from northwestern Maine. Am Mineral 62:438–448

Guidotti CV, Yates MG, Dyar MD, Taylor ME (1994) Petrogenetic implications of the Fe^{3+} content of muscovite in pelitic schists. Am Mineral 79(7–8):793–795

Henry DJ, Guidotti CV, Thomson JA (2005) The Ti-saturation surface for low-to-medium pressure metapelitic biotites: implications for geothermometry and Ti-substitution mecanisms. Am Mineral 90:316–328

Hermann J (2002) Experimental constraints on phase relations in subducted continental crust. Contrib Mineral Petrol 143(2):219–235

Hermann J, Spandler CJ (2008) Sediment melts at sub-arc depths: an experimental study. J Petrol 49(4):717–740

Hermann J, Rubatto D, Korsakov A, Shatsky SV (2001) Multiple zircon growth during fast exhumation of diamondiferous, deeply subducted continental crust (Kokchetav Massif, Kazakhstan). Contrib Mineral Petrol 141:42–66

Holland TJB, Powell R (1990) An enlarged and updated internally consistent thermodynamic dataset with uncertainties and correlations—the system K_2O–Na_2O–CaO–MgO–MnO–FeO–Fe_2O_3–Al_2O3–TiO_2–SiO_2–C–H_2–O_2. J Metamorph Geol 8(1):89–124

Holland TJB, Powell R (1998) An internally consistent thermodynamic data set for phases of petrological interest. J Metamorph Geol 16(3):309–343

Holland T, Powell R (2003) Activity-composition relations for phases in petrological calculations: an asymmetric multicomponent formulation. Contrib Mineral Petrol 145(4):492–501

Huang WL, Wyllie PJ (1973) Melting relations of muscovite-granite to 35 Kbar as a model for fusion of metamorphosed subducted oceanic sediments. Contrib Mineral Petrol 42(1):1–14

Huang WL, Wyllie PJ (1974) Melting relations of muscovite with quartz and sanidine in K_2O–Al_2O_3–SiO_2–H_2O system to 30 Kilobars and an outline of paragonite melting relations. Am J Sci 274(4):378–395

Lindsley DH, Nekvasil H (1989) A ternary feldspar model for all reasons. EOS Trans Am Geophys Union 70(15):506

Liu LG (2002) Critique of stability limits of the UHPM index minerals diamond and coesite. Int Geol Rev 44(9):770–778

Liu FK, Xua ZQ, Katayama I, Yang JS, Maruyama S, Liou JG (2001) Mineral inclusions in zircons of para- and orthogneiss from pre-pilot drillhole CCSD-PP1, Chinese Continental Scientific Drilling Project. Lithos 59(4):199–215

Liu FL, Xu ZQ, Liou JG, Katayama I, Masago H, Maruyama S, Yang JS (2002) Ultrahigh-pressure mineral inclusions in zircons from gneissic core samples of the Chinese Continental Scientific Drilling Site in eastern China. Eur J Mineral 14(3):499–512

Liu FL, Zhang ZM, Katayama I, Xu ZQ, Maruyama S (2003) Ultrahigh-pressure metamorphic records hidden in zircons from amphibolites in Sulu Terrane, eastern China. Island Arc 12(3):256–267

Liu FL, Xu ZQ, Liou JG (2004) Tracing the boundary between UHP and HP metamorphic belts in the southwestern Sulu terrane, Eastern China: evidence from mineral inclusions in zircons from metamorphic rocks. Int Geol Rev 46(5):409–425

Liu J, Ye K, Sun M (2006) Exhumation P–T path of UHP eclogites in Hong'an area, western Dabie Mountains, China. Lithos 89:154–173

Massonne HJ (2003) A comparison of the evolution of diamondiferous quartz-rich rocks from the Saxonian Erzgebirge and the Kokchetav Massif: are so-called diamondiferous gneisses magmatic rocks? Earth Planet Sci Lett 216(3):347–364

Massonne H-J, Schreyer W (1987) Phengite geobarometry based on the limiting assemblage with K-feldspar, phlogopite and quartz. Contrib Mineral Petrol 96:212–224

Montel JM, Vielzeuf D (1997) Partial melting of metagreywackes; part II, compositions of minerals and melts. Contrib Mineral Petrol 128(2–3):176–196

Nair R, Chacko T (2002) Fluid-absent melting of high-grade semipelites; P–T constraints on orthopyroxene formation and implications for granulite genesis. J Petrol 43(11):2121–2142

Parra T, Vidal O, Agard P (2002) A thermodynamic model for Fe–Mg dioctahedral K white micas using data from phase-equilibrium experiments and natural pelitic assemblages. Contrib Mineral Petrol 143(6):706–732

Patiño Douce AE, McCarthy TC (1998) Melting of crustal rocks during continental collision and subduction. In: Hacker BR, Liou JG (eds) When continents collide: geodynamics and geochemistry of ultrahigh-pressure rocks. Kluwer, Dordrecht, pp 27–55

Perier R (1999) Experimental melting of muscovite between 25 and 80 Kbar. Master thesis. Université Blaise Pascal, Clermont-Ferrand, France, p 18

Ringwoog AE, Lovering JF (1970) Significance of pyroxene-ilmenite intergrowths among kimberlite xenoliths. Earth Planet Sci Lett 7:371–375

Robert JL (1975) An experimental study of phlogopite solid solutions in the system K_2O–MgO–Al_2O_3–SiO_2–H_2O solubility of titanium in phlogopite solid solutions. Can Mineral 13(3):312

Robert JL (1976) Titanium solubility in synthetic phlogopite solid solutions. Chem Geol 17(3):213–227

Schmid R, Wilke M, Oberhaensli R, Janssens K, Falkenberg G, Franz L, Gaab A (2003) Micro-XANES determination of ferric iron and its application in thermobarometry. Lithos 70(3–4):381–392

Schmidt MW (1996) Experimental constraints on recycling of potassium from subducted oceanic crust. Science 272(5270):1927–1930

Schmidt MW, Vielzeuf D, Auzanneau E (2004) Melting and dissolution of subducting crust at high pressures: the key role of white mica. Earth Planet Sci Lett 228:65–84

Shatsky SV, Sobolev NV, Vavilov MA (1995) Diamond bearing metamorphic rocks of the Kokchetav Massif (northern Kazakhstan). In: Coleman RG, Wang X (eds) Ultrahigh-pressure metamorphism. Cambridge University Press, Cambridge, pp 427–455

Snoeyenbos DR, Williams ML, Hanmer S (1995) Archean high-pressure metamorphism in the western Canadian shield. Eur J Mineral 7(6):1251–1272

Sobolev NV, Shatsky VS (1990) Diamond inclusions in garnets from metamorphic rocks—a new environment for diamond formation. Nature 343(6260):742–746

Stevens G, Clemens JD, Droop GTR (1997) Melt production during granulite-facies anatexis; experimental data from "primitive" metasedimentary protoliths. Contrib Mineral Petrol 128(4):352–370

Storre B (1972) Dry melting of muscovite + quartz in range Ps = 7 kb to Ps = 20 kb. Contrib Mineral Petrol 37(1):87

Tracy RJ (1978) High grade metamorphic reactions and partial melting in pelitic schist, west-central Massachusetts. Am J Sci 278(2):150–178

Vavilov MA, Sobolev NV, Shatskii VS (1991) Micas from diamond-bearing metamorphic rocks of northern Kazakhstan. Dokl Akad Nauk Sssr 319(2):466–470

Velde B (1965) Phengite micas—synthesis stability and natural occurrence. Am J Sci 263(10):886

Vielzeuf D, Holloway JR (1988) Experimental determination of the fluid-absent melting relations in the pelitic system: consequences for crustal differentiation. Contrib Mineral Petrol 98(3):257–276

Vielzeuf D, Montel JM (1994) Partial melting of metagreywackes; part 1, fluid-absent experiments and phase relationships. Contrib Mineral Petrol 117(4):375–393

Waters DJ, Charnley NR (2002) Local equilibrium in polymetamorphic gneiss and the titanium substitution in biotite. Am Mineral 87(4):383–396

Watson EB, Wark DA, Thomas JB (2006) Crystallization thermometers for zircon and rutile. Contrib Mineral Petrol 151(4):413–433

Yang JJ (2003) Titanian clinohumite-gamet-pyroxene rock from the Su-Lu UHP metamorphic terrane, China: chemical evolution and tectonic implications. Lithos 70(3–4):359–379

Zanazzi PF, Pavese A (2002) Behavior of micas at high pressure and high temperature. In: Mottana A, Sassi FP, Thompson JBJ, Guggenheim S (eds) Micas: crystal chemistry and metamorphic petrology, vol 46. Mineralogical Society of America and Geochemical Society, Washington, DC, pp 99–116

Zhang RY, Hirajima T, Banno S, Cong B, Liou JG (1995) Petrology of ultrahigh-pressure rocks from the Southern Su-Lu region, Eastern China. J Metamorph Geol 13(6):659–675

Zhang RY, Liou JG, Ernst WG, Coleman RG, Sobolev NV, Shatsky VS (1997) Metamorphic evolution of diamond-bearing and associated rocks from the Kokchetav Massif, northern Kazakhstan. J Metamorph Geol 15(4):479–496

Zhang ZM, Xu ZQ, Xu HF (2000) Petrology of ultrahigh-pressure eclogites from the ZK703 drillhole in the Donghai, eastern China. Lithos 52(1–4):35–50

Zhang RY, Liou JG, Katayama I (2002a) Petrologic characteristics and metamorphic evolution of diamond-bearing gneiss from Kumdy-Kol. In: Parkinson CD, Katayama I, Liou JG, Maruyama S (eds) The diamond-bearing Kokchetav Massif, Kazakhstan; petrochemistry and tectonic evolution of an unique ultrahigh-pressure metamorphic terrane, vol 38. Universal Academy, Tokyo, pp 213–233

Zhang RY, Liou JG, Shu JF (2002b) Hydroxyl-rich topaz in high-pressure and ultrahigh-pressure kyanite quartzites, with retrograde woodhouseite, from the Sulu terrane, eastern China. Am Mineral 87(4):445–453

Zhang ZM, Xiao YL, Hoefs J, Xu ZQ, Liou JG (2005a) Petrogenesis of UHP metamorphic crustal and Mande rocks from the Chinese Continental Scientific Drilling Pre-pilot Hole 1, Sulu belt, eastern China. Int Geol Rev 47(11):1160–1177

Zhang ZM, Xiao YL, Liu FL, Liou JG, Hoefs J (2005b) Petrogenesis of UHP metamorphic rocks from Qinglongshan, southern Sulu, east-central China. Lithos 81(1–4):189–207

Zhang ZM, Shen K, Xiao YL, Hoefs J, Liou JG (2006a) Mineral and fluid inclusions in zircon of UHP metamorphic rocks from the CCSD-main drill hole: a record of metamorphism and fluid activity. Lithos 92(3–4):378–398

Zhang ZM, Xiao YL, Hoefs J, Liou JG, Simon K (2006b) Ultrahigh pressure metamorphic rocks from the Chinese Continental Scientific Drilling Project: I. Petrology and geochemistry of the main hole (0–2, 050 m). Contrib Mineral Petrol 152(4):421–441